



Quality assessment of multi-resolution DEMs for flood risk assessment purposes caused by extreme natural events: Application to the Bulgarian Black Sea Coast

Davis Dinkov¹, Lyubka Pashova¹

¹ National Institute of Geophysics, Geodesy and Geography - Bulgarian Academy of Sciences, Sofia, Bulgaria

Corresponding author: Davis Dinkov (davisdinkov@nauka.bg)

Abstract

High-resolution Digital Elevation Models (DEMs) are critical for accurate coastal flood risk assessment, particularly in low-lying areas vulnerable to sea-level rise, storm surges, and other natural hazards. This study presents a comparative evaluation of five DEMs with varying spatial resolutions and data sources for a test area along the northeastern Bulgarian Black Sea Coast around the Durankulak Lake—an area identified as at risk of coastal flooding. A high-resolution Uncrewed Aerial Vehicle (UAV) derived DEM was generated using Structure-from-Motion and Multi-View Stereo (SfM-MVS) photogrammetry and compared against three other DEMs: BG DSM (4 m), MGS DEM (10 m), and re-sampled TanDEM-X (10 m). The vertical accuracy of DEMs was assessed using control points (CPs), including GNSS-measured and geodetic reference points, and parametric and non-parametric statistical methods, along with statistical tests to assess the error distribution. Results indicate that the UAV and BG DSM models exhibited normal error distributions with high vertical accuracy (root mean square error: 0.098 m and 0.776 m, respectively), while the MGS and TanDEM-X models display significant deviations from normality and lower precision. The UAV-derived DEM has offered the highest accuracy and reliability, though it requires significant field and processing resources. The findings highlight the importance of selecting DEMs based on the required precision, available resources, and application-specific context, particularly for hydrologic and hydrodynamic modeling and flood risk mapping under the EU Floods Directive. This study provides a robust methodological framework for evaluating DEM quality and suitability in coastal hazard assessments and contributes to improved geospatial data practices in flood-prone regions.

Key words: Coastal flooding, coastal zone, Durankulak Lake, natural hazards, UAV photogrammetry, 3D terrain model

1. Introduction

Generation of a high-resolution Digital Topo-bathymetry Elevation Model (DT-BEM) is crucial for various coastal hazard applications, including flood prevention from storms, tsunamis, and sea-level rise (Jongman et al. 2012; Specht and Wiśniewska 2024). In the context of climate change and the increasing urbanization of the coastal zone, the hazards and risks associated with coastal flooding have significantly increased (Oppenheimer et al. 2019). The appropriate choice



This article is part of:
Methodological advances in geographical research
Edited by John Pickles, Chad Staddon

Academic editor: Galin Petrov
Received: 14 August 2025
Accepted: 12 March 2026
Published: 01 June 2026

Citation: Dinkov D, Pashova L (2026) Quality assessment of multi-resolution DEMs for flood risk assessment purposes caused by extreme natural events: Application to the Bulgarian Black Sea Coast. *Journal of the Bulgarian Geographical Society* 54: 201–232. <https://doi.org/10.3897/jbgs.e168786>

Copyright: © Davis Dinkov and Lyubka Pashova
This is an open access article distributed under terms of the Creative Commons Attribution License ([Attribution 4.0 International – CC BY 4.0](https://creativecommons.org/licenses/by/4.0/)).

of DTBEM for coastal hazard assessment depends on the scope and specific application for which it will be used (Guth et al. 2021). Its vertical accuracy varies widely across available models, methods for producing and combining data from different sources, and coastal zone features, due to differences in data quality, terrain, seabed relief, land cover, and numerous other factors.

More specifically, in coastal flood risk assessment, in addition to predicted water levels, a land Digital Elevation Model (DEM) is used to estimate potentially inundated areas and associated socio-economic damages. Coastal flood risk assessment is performed using a conceptual risk approach that uses Digital Elevation Models (DEMs) to assess flood hazard in coastal areas relative to predicted water levels (Nicholls et al. 2015). This assessment is significantly influenced by the resolution and accuracy of the DEM data, as elevation largely determines whether a location will be affected by flooding. Topographic data is the most critical factor in determining the extent of flooding and the accuracy of the flood forecast maps produced. In low-lying coastal areas and river deltas flowing into the sea, variations in elevation are of the order of several decimeters (Van de Sande et al. 2012). In the presence of errors of this magnitude in the topographic data, the accuracy of the risk assessment is significantly affected.

Available global DEMs with open access, such as the Shuttle Radar Topography Mission (SRTM), Advanced Spaceborne Thermal Emission and Reflection Radiometer (ASTER), Advanced Land Observing Satellite (ALOS), and TerraSAR-X add-on for Digital Elevation Measurements (TanDEM), are often utilized in coastal flood risk assessment studies, particularly in areas where such data are not readily available (Kulp and Strauss 2018; Hawker et al. 2019). Most freely available global elevation models are provided in grid form with a spatial resolution of 1 degree second, corresponding to 30 m at the equator. The quality of these DEMs in flood modeling has also been widely considered (Schumann et al. 2018). In many instances, the vertical accuracy of these DEMs is not regularly reviewed, assessed, or independently verified by comparing them with reference elevation models before they are used for coastal flood risk assessments. If errors exist in the elevation data, the accuracy of the risk assessment is significantly affected, potentially leading to overestimation or underestimation of the risk. Previous studies have noted that the openly accessible, widely used DEM, SRTM, was acquired in the 2000s and contains numerous errors (Hawker et al. 2018a, 2018b). Although constantly updated DEMs, such as Multi-Error-Removed Improved-Terrain (MERIT), NASADEM, EU-DEM, and CoastalDEM, have seen performance improvements, there are still regions of the world with complex and rugged topography that are not represented in sufficient detail and homogeneous height (vertical) accuracy (Uemaa et al. 2020; Gesch 2023; Guth et al. 2024; Ahmed et al. 2025). Several factors affect vertical accuracy, including physical limits of satellite sensing, vegetation and surface bias, terrain complexity, reference surface uncertainty, and cost and coverage trade-offs. In some cases, it has been shown that a particular DEM may underestimate or overestimate inundation areas and coastal exposure (e.g., Kulp and Strauss 2016; Becker et al. 2024).

High-resolution DEMs are essential for coastal hazard assessments, particularly for flood prevention at European and national levels. The choice of DEM product, such as the 10-meter EEA-10 or the 30-meter EU-DEM, significantly impacts the accuracy of hazard modeling outcomes. In the past two decades,

Europe has made strides in developing high-precision topographic and seabed models, supported by international initiatives. The European Environmental Agency maintains spatial data catalogues through the GMES RDA (EU-DEM) project (EU-DEM 2022), part of the Copernicus program. Key DEM products include the Digital Surface Model (DSM) and the Copernicus DEM (EEA-10) with a resolution of approximately 10 meters, covering the EEA-39 countries. Older products, such as the EU-DEM, are archived, and global versions, such as GLO-30 and GLO-90, are available. Countries like the Netherlands (Actueel Hoogtebestand Nederland 2025) and Belgium have effectively surveyed their territories using Light Detection and Ranging (LiDAR) technology.

In contrast, Bulgaria has yet to develop a comprehensive DEM/DSM that meets the necessary spatial and vertical resolutions for scientific tasks. Various institutes, research centers, and private companies maintain DEMs at different spatial resolutions. Some, like the Military Geographic Service (MGS) under the Ministry of Interior, offer services for a fee based on resolution and area. DEMs are usually provided in the WGS 84 coordinate system, with elevations referenced to mean sea level in the Baltic Height System or the EVRF2007 system. The Geodesy, Cartography and Cadastre Agency (GCCA) provides topographic data from 1:5000-scale maps, but these originals were created before the 1990s, potentially making them outdated for rapidly urbanizing areas. Data for models can be gathered using LiDAR, Unmanned Aerial Systems (UASs), or ultra-high-precision satellite images from commercial sources.

Scientific publications on DEM quality in Bulgaria are limited. Petrov (2013) analyzed a relief database from the MGS created between 1987 and 1992, which was based on medium-scale topographic maps and had an average height error of $\pm 3\text{--}5$ m. The data represent the “bare ground” and are generalized to the scale of the topographic maps, lacking detailed information about relief microforms.

Nikolov (2018) reviewed the history and application of DEMs in Bulgaria, while Pashova and Nikolov (2018) compared global DEMs (SRTM v.4.1 and ASTER GDEM v2) with a national DEM in Southwestern Bulgaria, finding that freely available models are only suitable for regional studies. Dinkov (2023) assessed the accuracy of high-resolution DEMs obtained from drone imagery, achieving vertical accuracy within 6–12 cm.

Based on the literature review of publications on DEM quality analysis in Bulgaria, most authors conclude that satellite DEMs (SRTM, ASTER) are convenient and freely available but have limited accuracy and are suitable only for coarse analyses, not for precise field studies. Historical local DEMs from the MGS (1987–1992) have an average accuracy of a few meters and are helpful for applied analysis over large areas, but are technologically outdated. Medium-scale DEMs are suitable for regional studies, whereas UAV-derived models offer the highest accuracy for engineering and environmental applications.

Over the past two decades, various remote sensing approaches with high spatial resolution, such as optical sensors on both airborne and space-based platforms, LiDAR operations, UASs, and video tracking systems, have been successfully applied to detailed mapping of coastal areas (Turner et al. 2016; Kakoulaki et al. 2021; Li et al. 2023; Shen et al. 2023; Sun et al. 2024). By applying these emerging technologies, a DEM can be generated with fine grids (1–5 cm) and high vertical accuracy (10–20 cm) (e.g., Uysal et al. 2015; Dinkov et al.

2023; Iqbal et al. 2023). These technologies are still used to a limited extent for mapping larger coastal areas due to their relatively high cost, specific image-acquisition conditions, and the need to process large data sets.

The accuracy of DEMs is crucial for implementing the EU Floods Directive (Directive 2007/60/EC), which aims to manage and reduce flood risks across Europe. Member States must assess watercourses and coastlines at risk of flooding, map potential flood areas, identify affected individuals, and take coordinated measures to mitigate these risks, using reliable data. DEMs are essential for mapping flood hazards, modeling flood behavior, and developing effective mitigation strategies. Inaccurate DEMs can lead to flawed flood risk assessments and inadequate management, especially as climate change increases the frequency of flooding.

In Bulgaria, the first Preliminary Flood Assessment in 2011 relied on a freely available 90-meter resolution SRTM DEM for coastal flood mapping due to the lack of a high-precision topographic model. However, studies have shown that this dataset's accuracy is relatively low, making it inadequate for detailed mapping (e.g., Pashova et al. 2017). During the second cycle of the Flood Directive (2022–2027), the National methodology for flood hazards and risk mapping (NMFHRM) was updated. This cycle involved revising Areas of Potential Significant Flood Risk (APSFR) and updating DEMs and flood hazard maps (MOEW 2023). Specifications for elevation accuracy in designated APSFR were defined, recommending various data sources for preparing high-accuracy DEMs (Dimitrov et al. 2013). Methods to enhance accuracy include using UAVs and LiDAR technology to create detailed 3D topographic models for coastal areas. Concerning flood hazard along the Bulgarian coast, flood hazard and risk maps for the Black Sea Directorate region have been developed for 34 significant flood risk areas, in line with updated assessment requirements (MOEW 2021). However, the NMFHRM does not explicitly outline necessary accuracy standards for DEMs used in hydrological modeling.

In recent years, UAS technology has proven to be a reliable method for creating orthophotomosaics and DEMs with higher spatial resolution and elevation accuracy at significantly lower cost than capturing areas for flood modeling (Annis et al. 2020; Karamuz et al. 2020; Prodanov et al. 2020). In general, different technologies for creating DEMs each have their pros and cons. For flood hazard and risk modeling, DEMs should have a horizontal resolution of at least 1 m x 1 m and a vertical accuracy better than 0.15 m according to the updated 2021 version of the Bulgarian NMFHRM (MOEW 2021). Airborne laser scanning and UAS mapping are recommended methods for obtaining accurate DEMs for flood hazard assessment. According to this methodology, compliance with Bulgarian legislation and regulations, especially Regulation No. RD-02-20-16, dated August 5, 2011, on aerial photography and remote sensing methods, is recommended for retention for coastal flooding mapping, as it currently does not meet national requirements for aerial UAV surveying.

Currently, DEMs with a spatial resolution of less than 1 m, suitable for detailed modeling of coastal inundation from natural hazard events such as storm surges, high winds coinciding with high tides, and tsunamis, can be generated from UAS imagery. Technological advances in UAS development and their increasing availability make them a cost-effective source for acquiring high-performance geospatial data in a relatively short time (Prodanov et al. 2023). The high spa-

tial resolution of the constructed 3D models of the captured objects (e.g., 0.05 m) is suitable for detailed studies of the coastal zone and various applications.

This study examines the qualities of five DEMs generated from different sources by comparing and evaluating descriptive statistics over the test area in the coastal zone of northeastern Bulgaria. We aim to 1) obtain a DEM generated by the UAV-SfM technique; 2) compare it with four DEMs with various spatial and vertical resolutions; 3) assess the vertical accuracy of each DEM using GCPs (Ground Control Points) measured by Global Navigation Satellite System (GNSS); 4) to provide recommendations when and what kind of DEMs may be used for different applications depending on purposes, e.g., for coastal flood modeling (due to sea storms, tsunami events, etc.) and risk assessment evaluation or other purposes. For research purposes, the quality and performance of DEMs are evaluated in the context of coastal flood risk assessment for one of the eight areas with potential sea flooding, specifically the Durankulak Lake area. To the best of our knowledge, this is the first attempt to compare the qualities of DEMs with relatively high spatial resolution from different sources, usable for coastal flood inundation modeling. Descriptions of the test area, used data, methodological approach, comparative analysis, and resulting findings are provided in the following sections.

2. Materials and methods

2.1. Case study area

As a test study region, we selected the Durankulak Lake region (Fig. 1), which is listed in the updated River Basin Management Plan and Flood Risk Management Plan for the Black Sea Region, Annex 10 (Black Sea Basin Directorate 2024). Due to the low-lying terrain, with an average elevation of approximately 30 meters (ranging from 0 m to 67 m a.m.s.l.), this region has historically suffered from coastal flooding. It is located in the Shabla Municipality, Dobrich District, of northeastern Bulgaria, and encompasses an area of 1,370.8 ha.

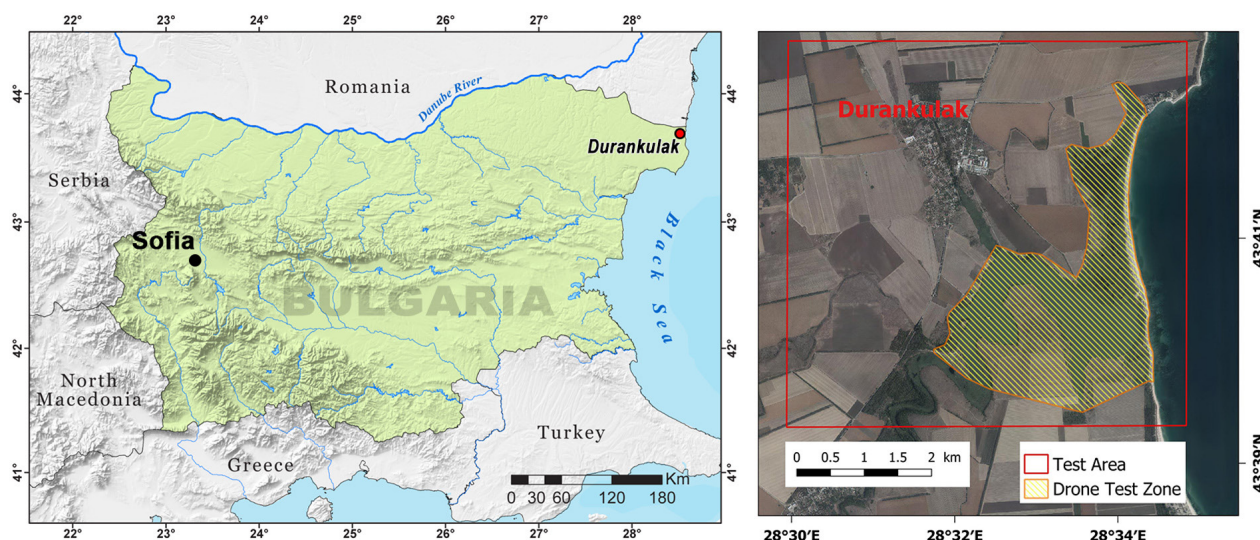


Figure 1. Case study area. **A** Location of the study area near the town of Durankulak within Bulgaria **B** Orthophoto image of the test site around Lake Durankulak (WGS'84: 43°40'N; 28°33'E).

According to national legal designations and the EU Natura 2000, this region is a Ramsar Convention site and is protected (MOEW 2016). Durankulak Lake is a shallow, brackish coastal wetland featuring open water areas dotted with dense reed beds and emergent aquatic plants, creating a visually rich water surface. The surrounding landscape comprises a mix of marshes, steppe vegetation, agricultural fields, and sand dunes, resulting in a diverse terrain shaped by both natural processes and human activity. The Lake spans 350 ha, and the region lies in a moderate coastal flood zone. The flood events occurred in association with various meteorological hazards, including prolonged rainfall and coastal flooding during severe storms. The coastal zone is characterized by a combination of dense, textured land and water, which exhibits significant variability in image characteristics and high illumination.

2.2. UAV DEM 0.5m/pixel

The UAV-DEM was derived using a photogrammetric approach, in which an RGB sensor captured overlapping images, which were then processed using the Structure-from-Motion (SfM) and Multi-View Stereo (MVS) workflows to create 3D point clouds (Iheaturu et al. 2020). These point clouds are used to generate 3D relief models of the Durankulak Lake region. The process follows a specific workflow outlined by Dinkov (2023), adhering to established guidelines for photogrammetric processing:

- Georeferencing: RTK GNSS positioning of the UAV images was used for cm-level georeferencing, and 1 GCP was used to correct elevation errors during the SfM-MVS model generation (Fazeli et al. 2016).
- UAV Navigation: The UAV's system records the camera's position in WGS84 geodetic coordinates (B, L, and h)—latitude, longitude, and geodetic height.
- Coordinate System: Photogrammetric points are expressed in WGS UTM 35N (flat coordinates) with altitude in the Baltic height system.
- GCP Measurement: GCPs are measured using GNSS RTK (accuracy of 2 cm at a 95% confidence level (Instruction No. RD-02-20-25/September 20, 2011) (MRDPW 2011)).
- Coordinate System Target: The study uses WGS UTM 35N for flat coordinates.
- Altitude Reference: Heights are referenced to the Baltic height system, which is still commonly used in Bulgaria's geodetic practices.
- Data Export: Results are exported in LAS (classified point cloud) and TIFF (numerical model and orthophotomap) formats.
- Image Resolution: The expected Ground Sampling Distance (GSD) is 4–5 cm/pixel, providing sufficient accuracy for generating high-precision digital terrain models (DTM) and point clouds for coastal zone analysis.

2.2.1. Field acquisition

The test area around Durankulak Lake was previously surveyed, and GCP locations were selected based on terrain features (Fig. 2A). Thirty-eight CPs, including 23 GNSS-measured points and 15 reference points from the state geodetic network (Fig. 2D–E), were used for all DEM comparisons. More concretely, for UAV DEM validation, we used 27 CPs: 22 GCPs measured by GNSS and 5 reference points from the state geodetic network, due to a smaller area captured

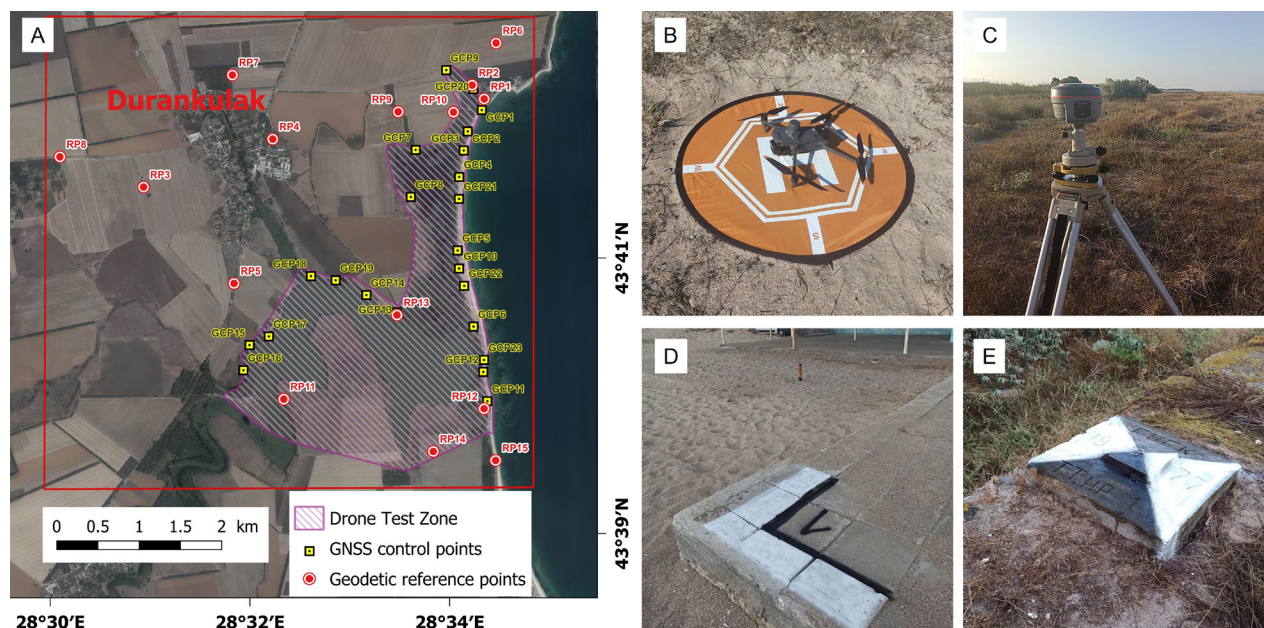


Figure 2. Test area surveyed by drone. **A** Studied area around Durankulak Lake with scheme of GCPs **B** UAV DJI Mavic 3M on takeoff/landing pad **C** Kolida K5 PLUS GNSS receiver **D** GCP mark **E** geodetic triangulation point marked as CP.

by UAV (Fig. 2B). One of the GCPs was removed from the validation points because it was used to generate the UAV-SfM model. The coordinates and heights of the GNSS points in the officially accepted coordinate and height systems used in Bulgaria were provided by the Geocartfund of GCCA (2023). The reference points were used to assess the accuracy of the DEM/DSM heights independently. Measurements were taken using a Kolida K5 PLUS receiver in RTK mode (Fig. 2C), offering high planimetric accuracy of 8 mm + 0.5 ppm Root Mean Square (RMS) and elevation accuracy of 15 mm + 0.5 ppm RMS. Coordinates were processed in the official Bulgarian geodetic coordinate system BGS2005 using BGSTrans ver. 4.6 software and transformed into the WGS 1984 (UTM zone 35N) and EVRF2007 height systems, with root mean square error (RMSE) in the range of ±0.8–5.2 cm in position and with RMSE of ±2–3 cm in height, respectively. For the study, all heights were further converted to the Baltic Height System to assess the vertical accuracy of various DEMs/DSMs.

A field UAV photogrammetric survey was conducted in July 2023 using a DJI Mavic 3M drone (Fig. 2B) over three days. The drone, a lightweight micro-class UAV (0.950 kg with RTK), was flown in automatic mode based on pre-planned flight paths. It features an integrated RGB camera and a multispectral sensor. The RGB camera is equipped with a 4/3 CMOS sensor with a 20MP resolution, a mechanical shutter, and a fast shooting interval of 0.7 seconds with lens characteristics: FOV: 84°, equivalent focal length: 24 mm, aperture: f/2.8 to f/11, focus: 1 m to ∞. The multispectral camera has a 1/2.8-inch CMOS sensor and 5 MP resolution with lens characteristics: FOV: 73.91°, equivalent focal length: 25 mm, aperture: f/2.0, fixed focus. Multispectral range of the cameras captures light across multiple discrete bands of the electromagnetic spectrum, namely: Green (G): 550 ± 16 nm; Red (R): 650 ± 16 nm; Red Edge (RE): 730 ± 16 nm; Near infrared (NIR): 860 ± 26 nm. Flights maintained 70% longitudinal and 80% traverse image overlap to ensure effective SfM processing. Ground control

targets were placed to enable accurate spatial validation of the resulting point cloud data. The PPK GNSS mode measurements were performed by onboard GNSS records, which track the position and altitude relative to the WGS ellipsoid. The GCPs' positions were determined relative to the Bulgarian BGS2005 coordinate system and the altitude relative to the Baltic height system. The camera's internal orientation parameters were taken from the photogrammetric software log file and optimized using automatic calibration during the pre-model development process (Table 1).

Table 1. Parameters for data acquisition using the DJI Mavic 3M.

Parameter	Value
Number of images	3777
Number of GCPs	23
Flight altitude	115 m
Average Ground Sampling Distance (GSD)	3.22 cm
RMSE	0.028 m
DSM and Orthomosaic resolution	5 cm/pixel
DTM resolution	50 m/pixel

2.2.2. Photogrammetric data processing and generation of topographic products

Photogrammetric processing of all images captured with the UAV was performed using Pix4D Mapper 4.5.6 software (Pix4D 2020). This program allows the creation of high-quality DSM, DTM, orthophotomaps, point clouds, and 3D models. A total of 3777 RGB images were processed, the coordinates of which were precisely determined in RTK mode with an average positional accuracy of ± 3.0 cm. When using UAV images captured in RTK mode, each image includes precise coordinates (latitude, longitude, and altitude) embedded in its EXIF metadata. In the SfM processing, only one ground point (GCP 18, Fig. 4A) was used to control vertical accuracy. The remaining 22 GCPs did not participate as controls in the photogrammetric processing but were used as validation points. When generating a dense point cloud (MVS workflow), a parameter was set to classify different land cover types automatically. The thus-classified dense cloud was used to create a DEM of the test area captured by the UAV.

The accuracy of the final raster photogrammetric products—orthomosaics, DEMs, and DSMs—was assessed using the open-source GIS software QGIS 3.34 LTR (QGIS Association 2023). QGIS was used for all data editing, analysis, visualization, and feature symbolization, resulting in thematic and topographic maps of the test area. The planimetric X and Y coordinates of the validation points were output to an external point shapefile, where the points represent the centers of the landmarks recognized in the orthophoto mosaic. Subsequently, Z coordinates were added for the vectorized points, using an additional tool (plugin) to extract Z values from the raster file (DSM/DTM). The coordinates thus obtained were exported to a text file and compared with the reference positions of the verification points. The planimetric accuracy of the digital model

derived from UAV imagery was evaluated using the $RMSE_{xy}$ of the validation point positions. The calculated planimetric accuracy is $RMSE_{xy} = \pm 2.88$ cm.

2.3. Digital Terrain Models of the studied area

Different types of geospatial data have been acquired, manipulated, and analyzed in the current study. Fig. 3 presents exemplary cropped DEM images that clearly depict the detailed topography of the relatively flat surface of the studied area. A grey scale was used to depict the topography, clearly expressing the roughness and complexity of the landforms in the study area for each DEM. The following sub-sections present characteristics of each data type. The georeferencing of all used data has been adjusted to the World Geodetic System 1984 (WGS84) UTM 35N as the horizontal datum, with the Baltic height system used as the vertical datum. We used one global TanDEM-X 30, two national DEMs with different spatial resolutions, and a high-resolution DEM produced from a UAV photogrammetric survey as the target for the accuracy assessments.

Table 2 presents the primary characteristics of the selected DEM datasets and provides an overview of each product in the subsequent sections. The following notations are used in this study: DEM refers to both DSM and DTM, where DSM represents the digital surface model (depicting natural terrain and artificial features), and DTM refers to the digital terrain model (“bare land”).

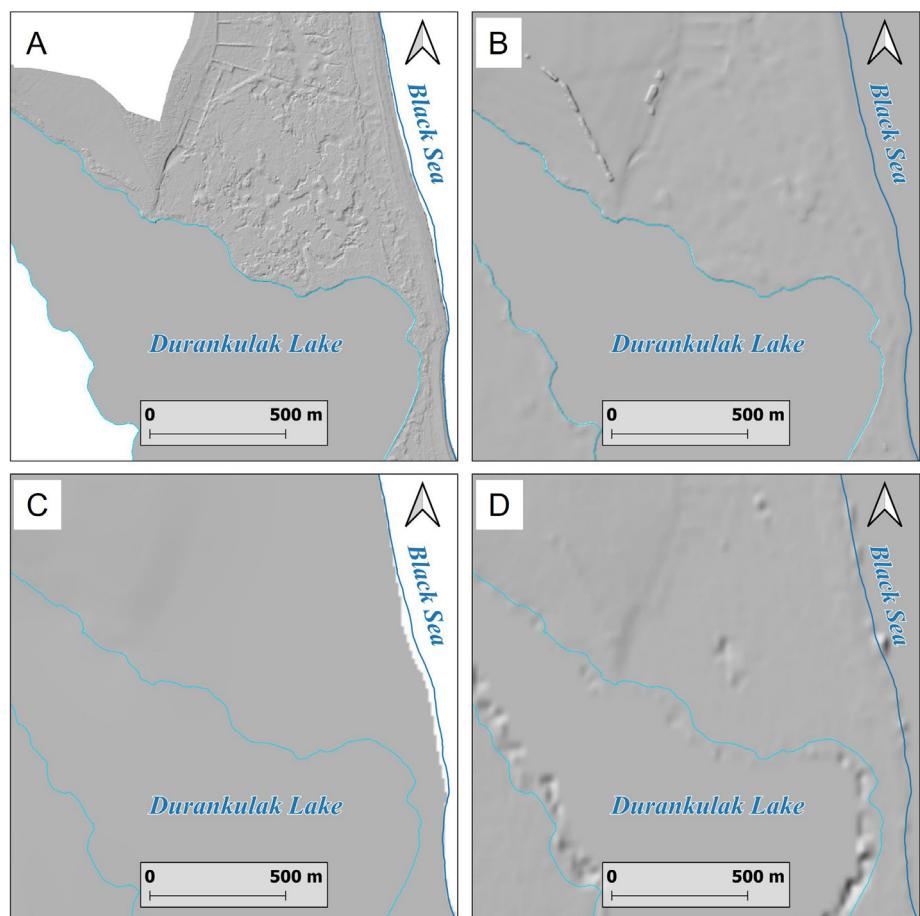


Figure 3. Images (extracts) of the test area from the four digital elevation models (DEM/DSM). **A** UAV DEM 0.5 m **B** BG DSM 4 m **C** MGS DEM 10 m **D** extrapolated TanDEM-X DEM 10 m.

Table 2. DEM datasets used in the study.

N	Data	Spatial resolution	Year of acquisition	Source	Type
1	MGS DEM	10 m	2015	Military Geographic Service	DSM
2	BG DSM	4 m	2022	Ministry of Agriculture and Food	DSM
3	TanDEM-X	30 m	2014	DLR	DSM
4	upsampledTanDEM-X	10 m	2014	DLR (resampling from TanDEM-X DEM 30 m)	DSM
5	UAV DEM	0.5 m	2023	Photogrammetrically derived from images captured by a UAV	DTM

2.3.1. MGS DEM 10 m

The Military Geographic Service requested MGS DEM (DTM) from the Bulgarian Army through the Ministry of Defence's geoportal (MD Portal 2025). The model was generated through photogrammetric processing in a grid with a 10 m spatial resolution, using scanned topographic maps at a scale of 1:25000. Heights are presented in the Baltic height system, with a "zero" point located at the tide gauge station in Kronstadt, Baltic Sea.

2.3.2. BG DSM 4 m

The BG DSM model, with a spatial resolution of 4 m, was provided by the Ministry of Agriculture and Food for research purposes. The model was generated as a by-product of photogrammetric processing of 2022 aerial imagery for the northern part of the Bulgarian territory (MAF 2024). Aerial photography is conducted periodically to update the country's digital orthophoto map, ensuring up-to-date land use data in the Land Parcel Identification System. The DSM is built relative to the WGS 84 coordinate system, and elevations are given in the Baltic height system or EVRF 2007 system.

2.3.3. TanDEM-X 30 m DEM

The TanDEM-X DEM was created using InSAR technology from TerraSAR-X and TanDEM-X satellite data, offering global coverage at spatial resolutions of ~12 m (scientific access), 30 m, and 90 m (freely accessible) (Wessel 2016; Wessel et al. 2018). It provides high-accuracy DSMs, with absolute vertical accuracy of up to 10 m (90% confidence) and relative accuracy of 2–4 m depending on slope (Zink et al. 2014; González et al. 2020). The DEM is referenced to the WGS84-G1150 ellipsoid and converted to orthometric heights using the EGM08 geoid with a 2.5 min cell size, in a common datum. For the Lake Durankulak study, a 30 m TanDEM-X tile in the projected coordinate system WGS 84/UTM zone 35N was used.

2.3.4. Extrapolated (upsampled) TanDEM-X 10 m DEM

To compare DEMs with as close as possible spatial resolutions, the original 30 m TanDEM-X model was upsampled to a 10 m cell size. Several test exper-

iments were conducted (not presented here) using different resampling methods on the original TanDEM-X 30-m grid to evaluate the accuracy of a 10-m resampled grid. Experiments showed that the accuracy of elevations remains unchanged under bicubic and bilinear interpolation when heights are extracted from the original model and transferred to the new model with higher spatial resolution. The 10-m model based on bilinear interpolation was used for further detailed analysis. In subsequent comparisons, both models, TanDEM-X 30 m and TanDEM 10 m, were utilized to demonstrate how the statistical estimates differ at 30 m and 10 m grid resolutions.

2.3.5. UAV-DEM

The classified dense point cloud from the SfM-MVS workflow was used to generate the UAV-DEM. The cloud was processed with the free software CloudCompare (CloudCompare project 2025), applying the CSF algorithm (Zhang et al. 2016) to generate the DEM using the “cloth simulation” technique (Weil 1986).

2.4. Data analysis techniques

To perform a comparative analysis of the selected DEMs, a methodological approach is proposed, followed by a step-by-step comparison and evaluation of the research models. When combining models with different spatial resolutions, it is necessary to consider the coordinate and axis systems used, the data format, whether the data can be processed using free or commercial software, and how well the software handles large data volumes. Fig. 4 illustrates the general workflow of the comparative study.

First, we extracted a DEM of the study test area within defined boundaries and transformed the coordinates and heights into the corresponding geodetic system. We employed two methods to process the DEMs. Before processing, resampling was performed to ensure consistent spatial resolution across the four datasets. Initially, TanDEM-X 30 datasets were downloaded and re-projected to the UTM coordinate system using the nearest-neighbor method, creating a 10x10 m grid in zone 35N, while maintaining the original data resolution (the original DEM’s pixel size is ~22 m at the test area’s latitude). For UAV-DEM, we resample it to 0.5 m resolution using bilinear interpolation. Secondly, all DEMs were converted to the same vertical datum by computing orthometric (normal) heights (H) (Table 3; see the original datum). For the standardization of the vertical datum, Eq. 1 is considered, where h is the value of the geodetic (geometric) height, N is the geoid height, given by the known value of the geoid undulation, and H is the orthometric (normal) height:

$$H = h - N \text{ (Eq. 1)}$$

Due to millimeter-level differences of 0 to 3–4 mm between orthometric and normal heights in the chosen Durankulak Lake test area (Belyashki and Mihaylov 2007), these were not further accounted for in the study and were therefore ignored. All DEMs are presented in the Baltic height system to ensure comparability by elevation. In addition to vertical standardization of the data, horizontal verification was performed by assessing the horizontal displacements

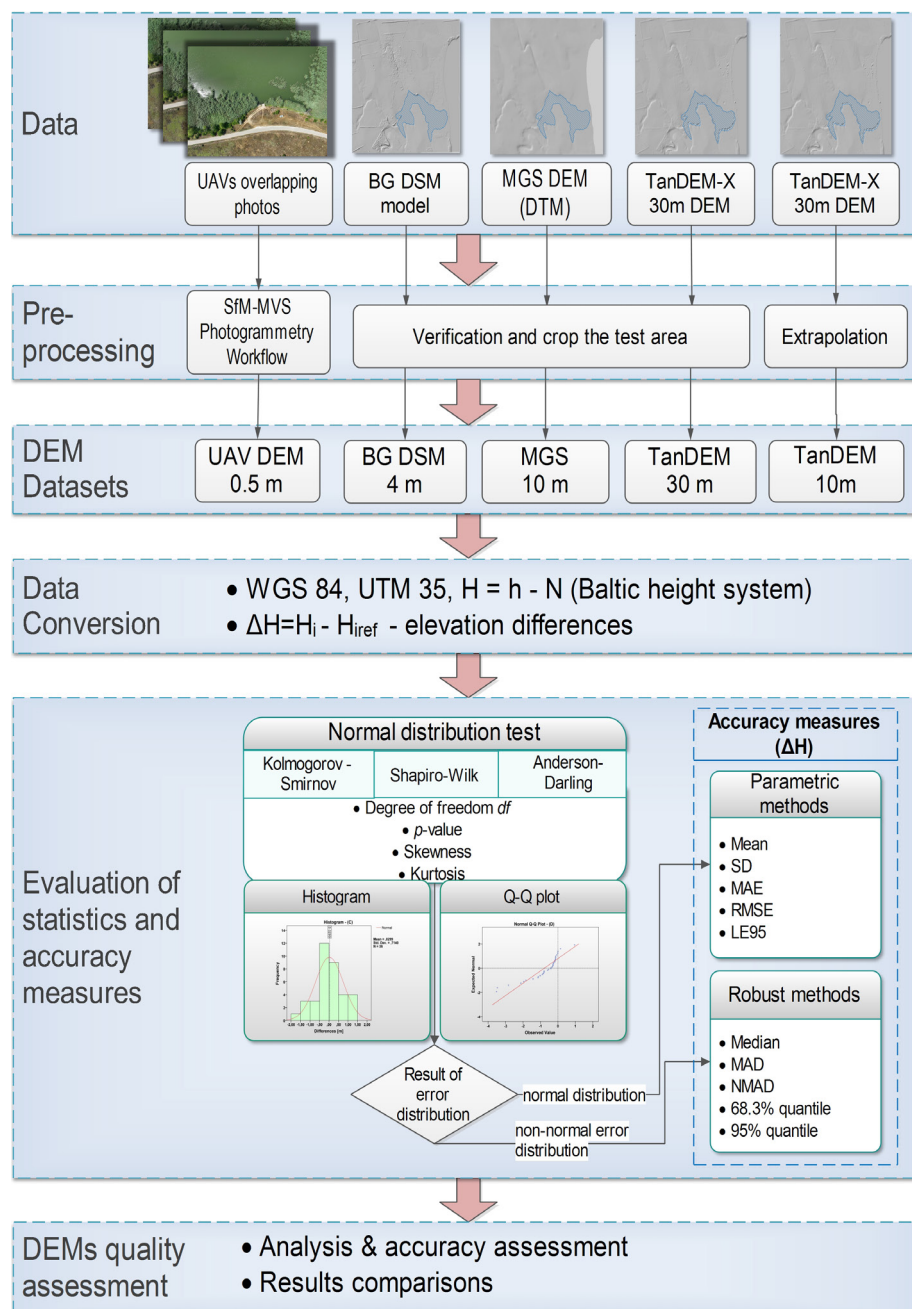


Figure 4. A workflow of the comparative analysis applied in this study.

of homologous features across the different DEMs. For horizontal adjustment, visual assessments were solely conducted. The transformations between the different coordinate and elevation systems, including UAV and various DEM data, were performed using the officially approved transformation program BGStrans ver.4.6, provided by the Geodesy, Cartography and Cadastre Agency (GCCA 2025). General characteristics of the five DEMs analyzed in this research are presented in Table 3.

To apply the Central Limit Theorem (CLT) for calculating statistical measures, such as the mean and standard deviation, the sample must have at least 30 points (Abdullah et al. 2024). When this condition is met, the sample mean is roughly normally distributed, allowing the use of the normal distribution to estimate uncertainty in population inferences.

Table 3. Digital elevation model (DSM/DTM) general characteristics.

DEM	Vertical Datum	Spatial resolution (pixel spacing) [m]	Acquisition method
UAV	Geodetic height	0.50	Photogrammetric SfM-MVS
BG DSM	Geodetic height	4	Photogrammetric
MGS	Normal height EVRF2007	10	Photogrammetric
TanDEM-X	Geodetic height Orthometric height	30/12	Interferometric (SAR)

Because different acquisition technologies use different sensors, some DEMs can produce more extreme errors in specific terrain types, skewing statistics and preventing a fair comparison if not removed. As a result, DEMs have different resolutions and noise characteristics. The vertical accuracy of five DEM datasets in this study was assessed by comparing their extracted heights with the corresponding elevations of reference (validation) points. For this purpose, the height differences ΔH between the DEM values reported with GNSS measurements of GCPs and the heights of the reference points from the state geodetic network were calculated using Eq. 2:

$$\Delta H = H_i - H_{iref} \text{ (Eq. 2)}$$

Where H_i is the elevation value obtained from the raster DEMs, H_{iref} is the reference value of the validation points that were measured by GNSS and extracted from coordinate registers. When comparing DEM elevations with GNSS-measured GCPs, positive height differences ($\Delta H = \text{DEM} - \text{GNSS} > 0$) indicate that the DEM overestimates elevation, meaning the surface is higher than the actual value. Conversely, negative height differences ($\Delta H = \text{DEM} - \text{GNSS} < 0$) indicate that the DEM underestimates elevation. Analyzing the overall distribution of these differences reveals systematic bias, random errors, and effects related to terrain or land cover. The height-difference datasets were then checked in two stages: first, the water-surface noise in the DEM was removed using the SAGA Fill Sinks algorithm in a GIS environment (Planchon and Darboux 2002). Then, the outliers were filtered using the three-sigma rule (Wessel et al. 2018). Outliers should be excluded when comparing DEMs for vertical accuracy, as they represent significant errors that can disproportionately skew statistical accuracy measures and obscure the true performance of the DEMs. Values outside the mean elevation difference (ΔH) plus/minus three times the standard deviation ($\Delta H > \Delta H + 3 * SD$, $\Delta H < \Delta H - 3 * SD$) were removed.

We employ various evaluation metrics to describe the distribution of DEM elevation errors. Each metric captures different aspects of elevation error, including bias, magnitude, variability, and extremes. No single measure can fully represent the overall quality of the DEM. The statistical indicators used in the study include mean value (MV), standard deviation (SD), RMSE, mean absolute error (MAE), median absolute deviation (MAD), normalised median absolute deviation (NMAD), and linear error at 95% (LE95) confidence level. Using these indicators, we obtained a quantitative evaluation of the distribution patterns of DEM elevation errors across different topographic characteristics in the studied region. Mean Error (ME) indicates the presence of bias in the data; MAE rep-

resents the average absolute magnitude of the elevation errors, ignoring their direction; and RMSE is sensitive to significant biases in the datasets (Carrera-Hernández 2021). It is worth mentioning that RMSE has some limitations as a measure of accuracy: a) it is based on a small sample of CPs, and b) it does not help determine whether the error is random, systematic, or gross (Wise 2000). The disadvantages of using CPs to validate DEMs are that they must be randomly distributed and represent a sufficiently large sample to obtain reliable accuracy estimates (Höhle and Höhle 2009). MAD and NMAD overcome these limitations due to their robustness and their propagation-free approach to handling data biases arising from possible heavy-tailed, non-normally distributed elevation differences (Höhle and Höhle 2009; Carrera-Hernández 2021).

To assess the accuracy of the DEMs compared to the reference elevations of the CPs, statistics are calculated according to the following equations (Eq. 3–5):

$$\text{MAE} = \frac{\sum_{i=1}^n (|\Delta H_i|)}{n} \quad (\text{Eq. 3})$$

$$\text{SD} = \sqrt{\sum_{i=1}^n \frac{(\Delta H_i - \Delta H)^2}{n-1}} \quad (\text{Eq. 4})$$

$$\text{RMSE} = \sqrt{\frac{1}{n} \sum_{i=1}^n (\Delta H_i^2)} \quad (\text{Eq. 5})$$

Where, ΔH means the height differences, and n is the number of validated CPs. RMSE is the root mean square of the mean elevation errors between the DEM and the corresponding reference values, and measures the overall accuracy of the DEM data. As the RMSE value approaches zero, the DEM-derived elevations are more accurate, while a greater distance from zero indicates a lower accuracy of the DEM-derived elevations.

Testing whether the height differences between CPs and a DEM follow a normal distribution is important. Many standard accuracy statistics and measures for DEMs, such as RMSE, SD and confidence levels, rely on the assumption of normal distribution. Verifying this assumption helps ensure that the accuracy assessments and interpretations of errors are statistically valid. The resulting height differences between those interpolated from the DEMs and the CPs' reference values are tested for normal distribution. To do this, the values of the statistical parameters skewness and kurtosis are calculated, and the Kolmogorov-Smirnov (K-S), Shapiro-Wilk (S-W), and Anderson-Darling (A-D) tests are also applied. Skewness measures the asymmetry of the distribution around the median, while kurtosis measures the intensity of the distribution (whether the data are peaked or flat relative to the normal distribution). K-S and S-W statistical methods, also known as non-parametric, compare an independent and identically distributed sample from an unknown univariate distribution of the analyzed sample with data from a reference distribution (Yap and Sim 2011). Specifically, the S-W test is beneficial and recommended for small sample sizes, as it provides greater power to detect deviations from normality (Höhle and Höhle 2009).

A comparative analysis of DEMs was performed, applying parametric and non-parametric statistical methods to the datasets: the elevation differences determined for CPs (GNSS-measured and geodetic reference points) and interpolated from each DEM by geographic coordinates. Additionally, to assess

the accuracy of each DEM regarding the representativeness of the depicted topographic relief, two topographic profiles were constructed and compared.

An alternative approach is needed to assess accuracy if asymmetry, kurtosis, or excessive deviations from a normal distribution are observed in a histogram of height differences. A robust approach that does not assume a normal error distribution, the study uses sample quantiles of the absolute elevation differences, $|\Delta H|$, focusing on the magnitude of the error rather than its direction. This method is robust to outliers and does not require a symmetric distribution. For datasets with a heavy-tailed error distribution, a more reliable scale estimator, such as the NMAD, is recommended for evaluating the spread of errors (Höhle and Höhle 2009). To analyze ΔH , we used the following equations (Eq. 6–7):

$$MAD = MD (|\Delta H_i - MD_{\Delta H_i}|) \quad (\text{Eq. 6})$$

$$NMAD = 1.4826 \times MAD \quad (\text{Eq. 7})$$

Where $MD_{\Delta H}$ is the median of the errors, indicating that NMAD is proportional to the median of the absolute difference between the errors and the median error. NMAD can be considered an estimate of the standard deviation that is more robust to outliers in the dataset. In the case of a normal distribution, this NMAD value is equivalent to the SD if the number of CPs is large enough (Höhle and Höhle 2009; Wessel et al. 2018). Usually, the sample size is deemed sufficient when it reliably represents the variability of the terrain and the distribution of errors. Generally, a minimum of 30 CPs is required for basic statistical validity. However, for a more robust accuracy assessment, especially across a range of slopes, land covers, and elevations, it's recommended to use 50 to 100, or more, CPs. In addition to non-parametric estimation, sample quantiles of the error distribution can also be used, where the quantile of a distribution is determined by the inverse of its cumulative distribution function (CDF), F , i.e., $Q(p) = F^{-1}(p)$. For normally distributed observations, a factor of 1.96 is applied to calculate the linear error (LE95) at the 95% confidence level (Greenwalt and Schultz 1962). Since height differences tend to follow a non-normal distribution, here LE95 is directly equivalent to the 95th percentile $\hat{Q}_{|\Delta H|}(0.95)$ of the sorted absolute differences calculated using the minimum rank method, i.e., the smallest value in the list. In other words, 95% of the data are less than or equal to this value (Eq. 8). To examine symmetry, a 68.3% error quantile $\hat{Q}_{|\Delta H|}(0.683)$, is also calculated, which, when compared with NMAD, should be identical; otherwise, it is an indication of a non-symmetric distribution.

$$LE95 = \hat{Q}_{|\Delta H|}(0.95) \quad (\text{Eq. 8})$$

In this study, we also used histograms and QQ-plots, which visually represent the frequency distribution of data and the distribution of a dataset against a theoretical distribution by plotting quantiles, respectively. These graphical methods help assess how well the data aligns with the expected normal distribution.

Following the proposed methodological approach described above, the pre-processing of selected DEMs for the test area around Lake Durankulak was performed. Second, the DEM data are transformed into the Baltic height sys-

tem. The selected locations of the chosen GCPs are measured in GNSS Real Time Kinematic (RTK) mode in static mode. Subsequently, these points and reference geodetic points are used to assess the accuracy of each of the five DEMs. The elevation differences are investigated by testing the hypothesis of normal distribution using parametric and non-parametric methods.

Furthermore, to evaluate the height accuracy of each DEM at various spatial resolutions, topographic profiles were created across the study area. These profiles provide a continuous representation of the terrain along selected transects, enabling direct and scale-independent comparisons of how elevation and landform shapes are depicted. They are particularly effective in revealing resolution-dependent effects such as smoothing, loss of detail, and distortion of terrain features, which are often overlooked by point-based accuracy metrics alone. Additionally, topographic profiles help identify systematic biases, spatial error patterns, and artifacts specific to each DEM. They emphasize how spatial resolution affects feature representation, effectively bridging the gap between point metrics and areal statistics. Moreover, these profiles allow for the assessment of gradients and terrain continuity, which are crucial for various geomorphological and hydrological applications. By linking simple statistical error measures with spatially explicit terrain analysis, profile-based comparisons provide an interpretable, reproducible, and physically meaningful approach to evaluating DEM performance across different resolutions.

3. Results

After preprocessing the four DEMs, their accuracy was evaluated using both parametric and non-parametric methods, as detailed in Section 2.4 and illustrated in Fig. 4. Initially, we performed a check for gross errors, removing any elevation difference values (ΔH) that exceeded three times the SD, as described in the procedure above. We then tested the ΔH differences for normal distribution by calculating several descriptive statistics and conducting the K-S, S-W, and A-D tests. The descriptive statistics for the five DEMs studied are summarized in Table 5. The distribution graphs, histograms, and Q-Q plots of the height errors for each DEM are displayed in Fig. 5. The histograms provide an initial indication of the distribution of errors. In contrast, the Q-Q plots, which compare the quantiles of the empirical data with the ideal distribution, provide a more comprehensive diagnostic for assessing deviations from normal distribution (Höhle and Höhle 2009).

The data for ΔH_{UAV} , as shown in the histogram in Fig. 5A, appear to be relatively close to a normal distribution. The mean is near zero, indicating minimal systematic bias, while the standard deviation of 0.09857 reflects the spread of the data. The Q-Q plot (Fig. 5B) further supports the assumption of normality, as the error distribution closely follows a normal distribution. Given this near-normal distribution, standard statistical measures such as mean and SD are appropriate. Additionally, Deviation (Dev) and RMSE can be utilized to assess accuracy.

The histogram of ΔH_{BG} DSM in Fig. 5C also suggests a relatively symmetrical distribution, with frequencies concentrated around the mean. A single negative value appears as an outlier in the left tail, but overall, there are no significant deviations from normality. The Q-Q plot (Fig. 5D) confirms that most data points align closely with the reference line, indicating an approximately normal

Table 5. Statistical parameters of height differences for control and reference points. Units (m).

Parameter	Descriptives					
	ΔH_{UAV}	$\Delta H_{BG\ DSM}$	ΔH_{MGS}	ΔH_{TanDEM}	$\Delta H_{TanDEM_{30}}$	
Mean	-0.01	0.30	0.03	-0.76	-0.86	
Std. error of mean	± 0.02	± 0.12	± 0.12	± 0.16	± 0.17	
95% Confidence Interval for mean	Lower bound	-0.05	0.06	-0.21	-1.11	-1.22
	Upper bound	0.03	0.54	0.27	-0.45	-0.51
5% Trimmed mean	-0.01	0.31	0.04	-0.71	-0.78	
Median	0.00	0.32	-0.02	-0.40	-0.61	
Variance	0.01	0.52	0.51	0.97	1.09	
Standard deviation (SD)	0.10	0.72	0.71	0.98	1.04	
Minimum	-0.19	-1.58	-1.78	-3.52	-4.01	
Maximum	0.16	1.93	1.41	0.95	0.62	
Range	0.35	3.52	3.20	4.47	4.63	
Interquartile range	0.17	0.92	0.37	0.93	1.10	
Skewness	0.15	-0.36	-0.31	-1.42	-1.43	
Std. error of skewness	± 0.45	± 0.39	± 0.39	± 0.39	± 0.39	
Kurtosis	-0.96	0.48	0.61	1.99	1.88	
Std. error of kurtosis	± 0.87	± 0.76	± 0.77	± 0.77	± 0.77	
RMSE	0.10	0.78	0.71	1.25	1.34	
LE95	0.19	1.52	1.38	2.44	2.64	
NMAD $ \Delta H $	0.13	0.65	0.26	0.58	0.63	
68.3% quantile $ \Delta H $	0.11	0.87	0.72	0.89	0.99	
95% quantile $ \Delta H $	0.16	1.40	1.38	2.99	3.41	

error distribution. A few points deviate on the left end of the plot, potentially representing outliers. Given the distribution's generally good shape, both standard and robust methods can be used to assess the accuracy of this DEM.

For ΔH_{MGS} , both the histogram and Q-Q plot in Fig. 5F support findings from non-parametric tests. The histogram (Fig. 5E) clearly illustrates a non-normal error distribution, with extended tails and noticeable outliers. The Q-Q plot reflects curvature in the central region and significant deviations, particularly in the lower-left corner, indicating that the data do not follow a normal distribution.

Regarding ΔH_{TanDEM} (Fig. 5G) and $\Delta H_{TanDEM_{30}}$ (Fig. 5I), the histograms show a distribution that is not symmetrical about the mean and exhibits skewness to the left (negative skew). There is a significant negative tail, with particularly noticeable values between -4.00 m and -3.00 m, indicative of anomalies (outliers). The deviation from a straight line on the Q-Q plot is apparent, especially on the left side, suggesting the presence of significant negative errors or a "heavy tail". The right side (positive values) shows a less pronounced deviation. In the central part of the Q-Q plot, the points are closer to the line; however, the overall distribution is not strictly linear. This visual analysis supports the hypothesis that the error distributions for TanDEM and TanDEM₃₀ deviate from the normal distribution.

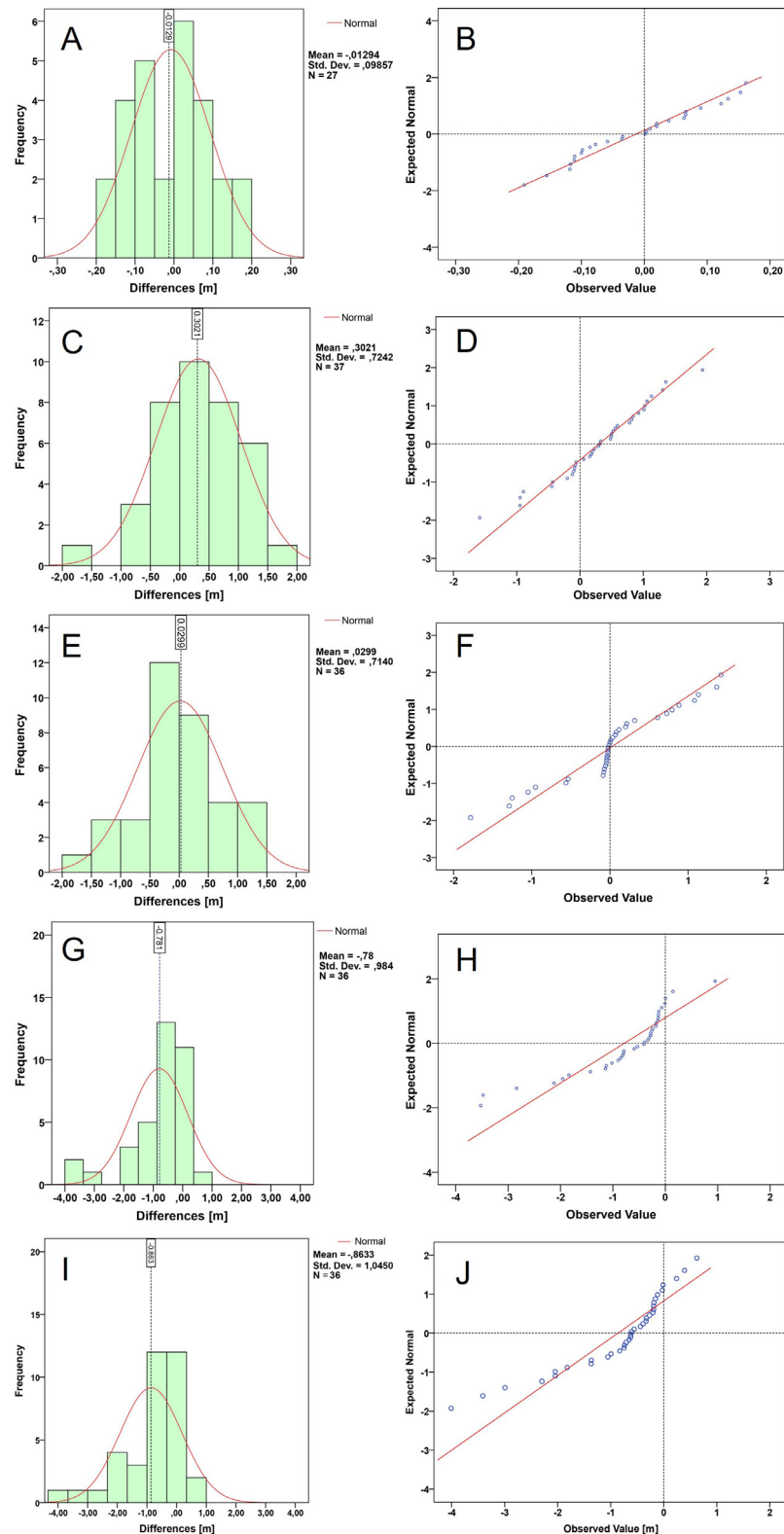


Figure 5. GNSS/Ref points error frequencies and Q-Q plots for the distributions ΔH , and superimposed curves in the histograms represent the normal distribution. **A** GNSS/Ref points error frequencies for ΔH_{UAV} **B** normal distribution for ΔH_{UAV} **C** GNSS/Ref points error frequencies for $\Delta H_{BG\ DSM}$ **D** normal distribution for $\Delta H_{BG\ DSM}$ **E** GNSS/Ref points error frequencies for ΔH_{MGS} **F** normal distribution for ΔH_{MGS} **G** GNSS/Ref points error frequencies for ΔH_{TanDEM} **H** normal distribution for ΔH_{TanDEM} **I** GNSS/Ref points error frequencies for $\Delta H_{TanDEM_{30}}$ **J** normal distribution for $\Delta H_{TanDEM_{30}}$.

Given the non-normal error distributions in the MGS and TanDEM, it is important to apply robust statistical methods that are less sensitive to outliers and deviations from normality. In addition to standard statistics, we calculated the NMAD and the 68.3% and 95% quantiles of absolute errors for each surface, as shown in Table 5. Comparing results from standard and robust methods allows for an evaluation of how non-normality and outliers affect accuracy estimates.

Based on hypothesis testing and visual analysis of the histogram and Q-Q plot, the differences between the drone DEM and GCPs follow a normal distribution. The RMSE (0.10 m) and SD (0.10 m) are identical, as are the mean and median values, which are also closely aligned. This result indicates minimal or no systematic bias. The similarity between SD and NMAD (0.13 m) suggests that outliers have little impact on the results. Approximately 68% of the absolute errors are below 0.11 m, and 95% are below 0.16 m, indicating good overall accuracy for this DEM surface.

The error distribution for the BG DSM-DEM model is approximately normal, as confirmed by hypothesis testing and visual assessments using histograms and Q-Q plots. The RMSE (0.78 m) and SD (0.72 m) are close, pointing to low systematic bias. A slight difference between the mean (0.30 m) and median (0.32 m) may suggest minor systematic bias. Robust statistical analysis indicates that the SD (0.72 m) is greater than the NMAD (0.65 m), suggesting the presence of outliers. About 68% of absolute errors are below 0.87 m, and 95% are below 1.40 m.

For the MGS-DEM, both hypothesis testing and visual inspection of histograms and Q-Q plots confirm a deviation from normality in the error distribution. Consequently, robust methods are necessary for an accurate and reliable assessment. The difference between the mean (0.03 m) and median (-0.02 m) is small, and the mean is close to zero, suggesting there is no significant systematic error. However, the SD (0.71 m) is considerably larger than the NMAD (0.26 m), indicating a wide dispersion caused by outliers. Approximately 68.3% of the absolute errors fall below 0.72 m, while 95% are below 1.38 m.

Similarly, the error distributions for TanDEM-DEM and TanDEM_30 show deviations from the normal distribution, as confirmed by three statistical tests and visual inspections of histograms and Q-Q plots. Therefore, robust measures such as NMAD and quantiles are more suitable for evaluating accuracy. As shown in Table 5, the significant difference between the mean (-0.76 m) and median (-0.40 m) suggests a potential systematic shift. The SD (1.23 m) is considerably larger than the NMAD (0.53 m), indicating a strong influence from outliers. Approximately 68.3% of absolute errors are below 0.89 m, and 95% are below 2.99 m. These findings reflect the characteristics of the error distribution for the TanDEM model in the test area.

In Table 6, the results of the normal distribution tests are presented using the K-S, S-W, and A-D tests. The degrees of freedom (DF), correspond to the relevant sample size indicated by n when checking the statistical tests. The test results indicate that the height differences between the drone and BG DSM DEMs are normally distributed, as evidenced by a p -value greater than 0.05. The results of the normality tests showed that the elevation differences for three of the DEMs, namely ΔH_{MGS} , ΔH_{TanDEM} , and $\Delta H_{\text{TanDEM}_{30}}$, do not support the hypothesis of normal distribution. The null hypothesis of normality is rejected when the p -value is less than or equal to 0.05, which is indicated

by the underlined values in the corresponding cells for the MGS, TanDEM, and TanDEM_30 models. Of the total number of evaluated height differences, 39, of which, due to outliers, 2 differences were removed for DH_BG DSM and 3 values respectively for ΔH_{MGS} , ΔH_{TanDEM} and $\Delta H_{TanDEM_{30}}$. The smaller number of height differences ΔH_{UAV} analyzed is due to the smaller captured area by the UAV compared to the DEM models. The conclusions after the performed analyses and comparisons remain unchanged.

Table 6. Tests for normal distribution.

Tests	Parameter	dz_DEM model dataset				
		ΔH_{MGS}	ΔH_{UAV}	$\Delta H_{BG\ DSM}$	ΔH_{TanDEM}	$\Delta H_{TanDEM_{30}}$
Kolmogorov-Smirnov	Statistic	0.240	0.114	0.090	0.205	0.177
	Degree of freedom (DF)	36	27	37	36	36
	p-value	0.000	0.200	0.200	0.006	0.005
Shapiro-Wilk	Statistic	0.924	0.963	0.98	0.856	0.862
	Degree of freedom (DF)	36	27	37	37	37
	p-value	0.017	0.426	0.803	0.000	0.001
Anderson-Darling	AD stat	1.388	0.393	0.274	2.202	1.688
	p-value	0.0014	0.377	0.665	0.000	0.0003
	crit value	0.735	0.728	0.735	0.734	0.735

We also provide a box-and-whisker plot in Fig. 6 that summarizes the height differences data samples' visual description, showing the median, quartiles, and available outliers. As shown in the figure, ΔH_{MGS} and ΔH_{UAV} have similar MAE values but different quartiles and outliers in the former; the other three DEMs have a more pronounced quartile range and a greater number of outliers, as ΔH_{MAF} has a positive MAE compared to the negative for both ΔH_{TanDEM} s. Interestingly, the height differences for the upscaled ΔH_{TanDEM} model have lower MAE and 3rd-1st quartile ranges than for the original $\Delta H_{TanDEM_{30}}$, but the min-max ranges are almost the same.

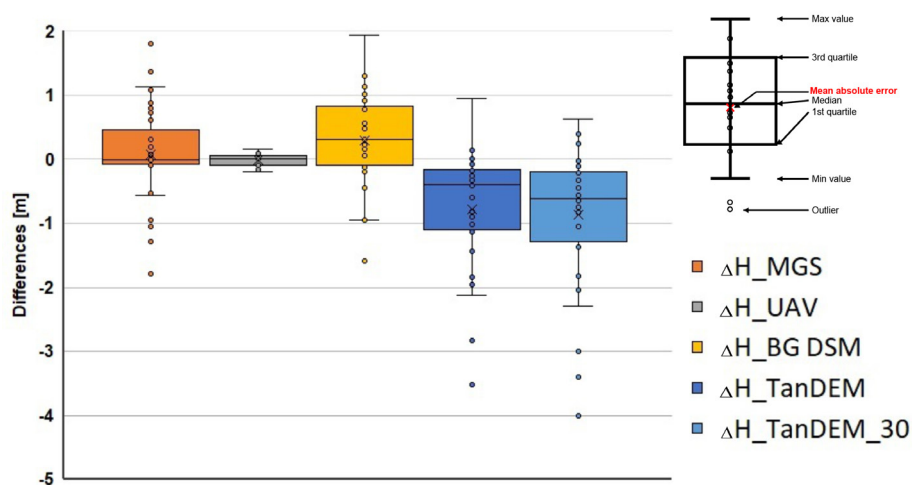


Figure 6. Comparison of elevation differences for the five DEMs using a boxplot.

Based on the comparative analysis and results shown in Table 5 and Figs 5, 6, we can conclude that the error distribution of elevation differences ΔH_{UAV} is nearly normal, with minimal bias (mean ≈ 0) and low dispersion (SD ≈ 0.10 m). Outliers have little impact (SD \approx NMAD), indicating high accuracy and reliability. ΔH_{BG} DSM: Distribution is roughly normal with a slight negative outlier. Small bias (mean \approx median) and moderate spread (SD = 0.72 m). Some outliers exist (SD > NMAD), but accuracy remains acceptable. The error distribution of ΔH_{MGS} is clearly non-normal, with extended tails and outliers. Low bias, but large SD (0.71 m) compared to NMAD (0.26 m), indicating high variability and sensitivity to outliers. The ΔH_{TanDEM} and ΔH_{TanDEM}_{30} differences exhibit a strongly non-normal distribution with long tails, particularly on the negative side, biases—mean values of -0.76 m and -0.86 m vs. median values of -0.40 m and -0.61 m, high dispersions—SD of 0.98 and 1.04 m, NMAD values of 0.58 m and 0.63 m, respectively.

In addition, to compare the four DEMs, we built two profiles: one that crosses Durankulak Lake in a southwest-northeast direction, profile "A", and the second profile "B" that is along the coastline in a north-south direction (Fig. 7). These profiles, the first with a 3100 m length and the second with a 2900 m length, are shown in Fig. 8 and Fig. 9, respectively.



Figure 7. Profile lines used for comparisons of the four DEMs. GNSS control points (GCP) are marked with red squares, and geodetic reference points (RP) are marked with a yellow triangle.

Comparing the elevations per profile "A", it is evident that three of the models—drone, BG_DSM, and TanDEM—realistically represent the Earth's surface, despite the first being a DTM and the other two being DSMs. The most significant overlap is observed between the UAV-DEM-generated model and the Ministry of Agriculture and Food, with resolutions of 0.5 m and 4 m, respectively. This result is to be expected, as these models are derived from modern measurements, the first from 2023 and the third from aerial photography in 2022. The elevations from the

TanDEM model also follow the land surface, with some underestimation of the heights in the marshy area of Lake Durankulak approaching the Black Sea water-line. The profile “A” from the MGS model shows that the surface is quite smooth, although there is some overlap in small areas. A possible explanation is that photogrammetric processing of medium-scale maps at 1:25000 and 1:50000 scales often fails to capture fine-scale detail, which has not been updated or renewed by geodetic surveying or other data sources in recent years.

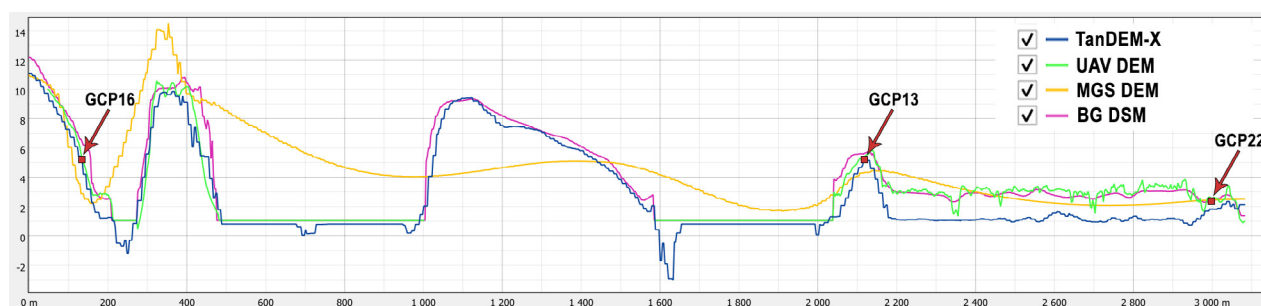


Figure 8. Profile line “A” shown in Fig. 7 in the SW–NE direction.

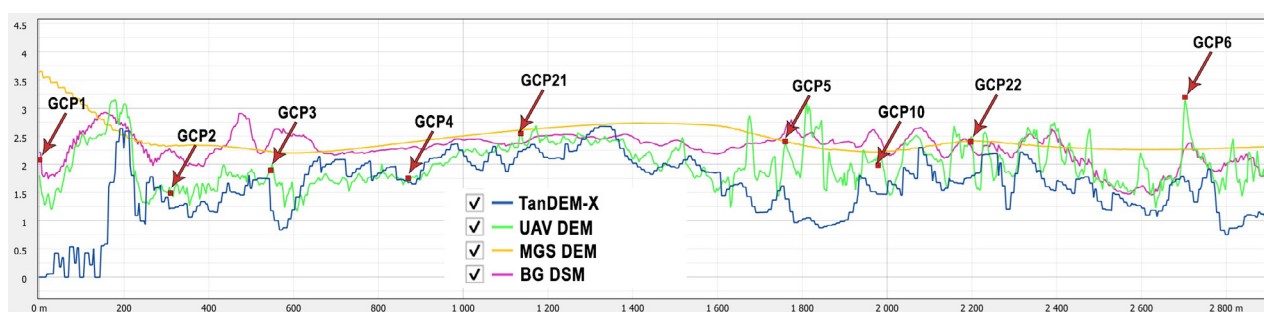


Figure 9. Profile line “B” shown in Fig. 7 in the N–S direction along the coastline with marked GCPs.

When comparing the elevations in profile “B” along the coastline, it is found that there is a relatively good correspondence between the drone and TanDEM models, with some systematic lowering in the second model at the southernmost and northernmost parts of the profile. However, systematic biases remain, particularly at edges or in zones of unique land cover in low-lying coastal areas, confirming that even advanced global DEMs can exhibit localized vertical deviations (e.g., Emmendorfer et al. 2024). The other two models, BG DSM and MGS, exhibit a relatively smooth topography, as shown in the MGS model.

4. Discussion

In this study, we compared five DEMs of the Durankulak Lake test area, obtained using different technologies and processing methods, following the proposed methodological approach shown in Fig. 1. The high spatial resolution achieved through photogrammetric UAV imaging directly impacts the accuracy of the DEM derived in this study, enabling a more accurate representation of the topographic characteristics of the test area. Accordingly, the flat relief is presented in greater detail, and the elevations are determined with higher accuracy than in the other three DEMs, as shown in Fig. 3. Both the BG DSM and

the map-derived MGS models show relatively smooth terrain representations, lacking the microtopographic variability present in UAV datasets.

The comparative analysis reveals apparent differences in accuracy and error behavior among the evaluated DEMs. The UAV DEM exhibits a near-normal error distribution with negligible bias, very low dispersion, and minimal influence of outliers, indicating the highest accuracy and reliability. The BG DSM DEM also shows an approximately normal distribution with moderate dispersion and a small systematic bias, yielding acceptable overall accuracy despite some outliers. In contrast, the MGS DEM demonstrates a clearly non-normal error distribution with extended tails and outliers, where low mean bias is offset by high variability and reduced robustness. Robust statistical measures (NMAD and error quantiles) are therefore more appropriate for MGS and TanDEM products, whereas parametric metrics are suitable for UAV and BG DSM DEMs. Overall, the UAV DEM performs best, followed by BG DSM, whereas MGS and, especially, TanDEM-based models show lower reliability due to non-normality and outlier sensitivity.

We also found that individual local topographic features (e.g., small depressions, gullies, planted crops, embankments, the presence of vegetation on the lake shore, and artificial structures), even in the more detailed and highly accurate UAV-DEM-generated model, can lead to height errors of 1–2 m in the final model, which requires additional verification with independent reference data. Although the study area of Durankulak Lake is relatively flat, during photogrammetric processing of the initial point cloud, local extremes were identified as anomalies caused by artificial small objects. Subsequently, through interpolation and filtering techniques, these local extremes were removed and controlled by accurate integration with GCPs and from the field survey data, which enabled cross-validation and ensured the correct modeling of individual topographic features to achieve good global accuracy.

The results show that the UAV-derived DEM has the highest accuracy and reliability, characterized by a nearly normal error distribution, negligible bias, low dispersion, and minimal influence of outliers. The BG DSM demonstrates acceptable accuracy with a roughly normal distribution and moderate variability, though some outliers affect its spread. In contrast, the MGS DEM exhibits a non-normal error distribution with pronounced outliers and high variability, indicating lower reliability despite its low mean bias.

Several studies have systematically compared the accuracy of the TanDEM-X DEM with reference sets from other global models against high-resolution reference datasets (Wessel 2016; Wessel et al. 2018; Bueso-Bello et al. 2021; Pronk et al. 2024; Velegrakis et al. 2024). Like any global product, TanDEM-X datasets contain biases and artifacts, with most global DSMs tending to overestimate elevation in forested and urban areas due to errors of omission. Zhang et al. (2019) demonstrated that TanDEM-X vertical accuracy varies by terrain type and that it exhibits larger vertical errors in vegetated and wet areas than in open ground, particularly when validated against airborne LiDAR benchmarks. Brosens et al. (2022) showed that, compared with a high-resolution UAV DEM, TanDEM-X underestimates the volumes of small erosional features due to its lower resolution. The TanDEM model generally captures surface elevations well, but it tends to underestimate heights in wet, marsh-like zones, low-lying areas, and vegetated environments, where radar penetration and scattering can bias elevation values (Zhang et al. 2019; Lee and Hong 2024).

For Durankulak Lake, we found that grid cells immediately adjacent to the Black Sea coastline lack elevation values in the original TanDEM-X product file (EOC Geoservice 2025). Upscaling TanDEM data slightly improves central accuracy (lower MAE and interquartile range), but extreme errors remain essentially unchanged, as shown by similar min–max ranges. This indicates that resampling reduces noise in the central distribution but does not eliminate large systematic or terrain-related errors. The TanDEM-X and TanDEM-X 30 m DEMs exhibit the poorest statistical behavior among the datasets compared, with strongly non-normal error distributions, pronounced negative biases, and long tails dominated by outliers. The large differences between mean and median values, together with high SD relative to NMAD, indicate that a few extreme errors substantially influence conventional accuracy measures. Consequently, as noted by Höhle and Höhle (2009) and Carrera-Hernández (2021), robust statistics are crucial, especially for small samples, to obtain reliable and representative accuracy estimates.

The selected control points for constructing the two profiles fall within corresponding pixels with different integral heights in each DEM, demonstrating the representativeness of the respective elevation models. The main sources of error when comparing high-precision GNSS-measured GCPs with DEMs at different resolutions (0.5 m, 4 m, 10 m and 30 m) are determined by the scale, generalization, and interpolation methods. In this study, the selection of GCP locations is tailored to bare ground. Spatial aliasing error is due to the pixel size, and the larger the pixel size, the more the terrain is smoothed. In this case, the UAV DEM captures the microrelief, and errors are minimal, whereas in 10 m or 30 m cell-resolution DEMs, larger errors are observed (i.e., differences in height relative to the GCPs). The errors can also be due to horizontal pixel displacement (Registration error) for the different models. In the present study, it was found that the BG DSM models with a cell size of 4 m and TanDEM-X with a cell size of 30 m significantly better represent the topographical surface, whereas the MGS DEM with a cell size of 10 m does not.

Although the use of high spatial and elevation resolution imagery from UAVs is one of the best data sources for creating high-accuracy topographic DEMs of low-lying coastal areas, many factors should be considered, such as cost, time available for field survey, post-processing of large volumes of data with specialized software, and available research infrastructure. For specific applications, such as marine flooding caused by storm surges or tsunami waves triggered by earthquakes, a preliminary assessment of the accuracy of any model to be used in subsequent modeling or simulation studies should be conducted.

The acquisition and provision of high-accuracy DEMs depend on several factors, such as sensor type, spatial resolution, coverage area, licensing restrictions, and the complexity of workflows for processing large volumes of data. Pre- and post-processing requirements (radiometric correction, co-registration, noise filtering, terrain modeling, and verification) vary significantly depending on whether the source data comes from optical, LiDAR, radar, or photogrammetric methods, sensors used and for what applications they are intended. When updating DEMs, differences in sensor characteristics, data-collection geometry, and changes over time should be taken into account. The diverse applications of these models require ensuring consistent accuracy and integration of datasets captured with different technologies.

5. Conclusion and future directions

This study investigates the qualities of four DEMs with different spatial and height resolutions and their usability for coastal flood risk assessment in a low-lying test area along the Bulgarian Black Sea Coast. A photogrammetric survey of the potentially threatened area around Lake Durankulak in northeastern Bulgaria, identified as being at risk from coastal flooding, was conducted to obtain a highly accurate UAV-based terrain model. The resulting high-precision DEM, together with the other three DEMs with different spatial resolutions (BG DSM, MGS, and TanDEM), was systematically analyzed and compared with GCPs to assess their accuracy and representativeness for the test area with flat topography using a proposed methodological approach comprising sequential steps. The results indicate that two of the DEMs, drone-generated and BG DSM, exhibit normal distribution characteristics, whereas this was not established for the other two, MGS and TanDEM. There are differences in the magnitudes of height error and relief representation between the four DEMs for the local study area, which should be considered when using the models for different applications. The choice of DEM source depends on the required accuracy and available resources. For small areas, it is advisable to use UAVs for a detailed survey. Although the study area of Durankulak Lake is relatively small, the resampled TanDEM model with a 10x10 m grid exhibits good height accuracy, despite some systematic deviations of approximately 2–3 m in specific local regions. The declared relative accuracy of the TanDEM heights is of the order of 2 m (Wessel et al. 2018), which was confirmed for this area by the present analysis of vertical accuracy.

In a future study, it is planned to investigate and assess the accuracy of the freely available EU-Copernicus DEM 30 m for a larger area of the Bulgarian territory, covering different topographic landforms. It is of scientific interest to perform a comparative analysis between different freely available DEMs and to assess their accuracy (e.g., Hawker et al. 2022; Meadows et al. 2024), as well as to perform a reliable validation using high-precision reference models, such as Airborne LiDAR or acquired via UAV and control geodetic points, especially in the complex transitional zones along the Bulgarian coast. Such an assessment is crucial for improving hydrodynamic flood models, where even decimeter vertical deviations can significantly change the predicted flood extents in low-lying coastal areas.

The results of this study provide valuable information for selecting and developing similar DEMs for coastal areas, offering a scientific basis for comparative studies of the elevation accuracy of photogrammetrically derived UAV, aerial, and satellite 3D models of Earth's surface.

Acknowledgements

The authors express their gratitude to Dr. Atanas Kitev, who participated in the field survey of the study area. They are grateful for the free provision of topographic data from the Geodesy, Cartography and Cadastre Agency, for the DEM 4m model from the Ministry of Agriculture and Food and for the free accessible TanDEM-X 30 m provided by the Earth Observation Center (EOC) of the German Aerospace Center (DLR). Finally, the authors would like to thank the anonymous reviewers for their valuable comments and suggestions to improve this manuscript.

References

- Actueel Hoogtebestand Nederland (2025) Dataroom <https://www.ahn.nl/dataroom> [Accessed on 11.12.2025]
- Ahmed M, Titti G, Trevisani S, Borgatti L, Francioni M (2025) Is higher resolution always better? A comparison of open-access DEMs for optimized slope unit delineation and regional landslide prediction. *Natural Hazards and Earth System Sciences* 25: 2519–2539. <https://doi.org/10.5194/nhess-25-2519-2025>
- Annis A, Nardi F, Petroselli A, Apollonio C, Arcangeletti E, Tauro F, Belli C, Bianconi R, Grimaldi S (2020) UAV-DEMs for Small-Scale Flood Hazard Mapping. *Water* 12(6): 1717. <https://doi.org/10.3390/w12061717>
- Abdullah Q, Munjy R, Nimetz J, Zoltek M, Lee C (2024) ASPRS Positional Accuracy Standards for Digital Geospatial Data. ASPRS, 228 pp. <https://doi.org/10.14358/ASPRS.PAS.2024>
- Becker M, Seeger K, Paszkowski A, Marcos M, Papa F, Almar R, Bates P, France-Lanord C, Hossain MS, Khan MJU, Karegar MA, Karpytchev M, Long N, Minderhoud PSJ, Neal J, Nicholls RJ, Syvitski J (2024) Coastal Flooding in Asian Megadeltas: Recent Advances, Persistent Challenges, and Call for Actions Amidst Local and Global Changes. *Reviews of Geophysics* 62(4): e2024RG000846. <https://doi.org/10.1029/2024RG000846>
- Belyashki T, Mihaylov E (2007) Determining the difference between the heights of the geoid and quasi-geoid for the territory of Bulgaria. *Geodesy, Cartography and Land Management* 5–6: 4–6.
- Brosens L, Campforts B, Govers G, Aldana-Jague E, Razanamahandry VF, Razafimbelo T, Rafolisy T, Jacobs L (2022) Comparative analysis of the Copernicus, TanDEM-X, and UAV-SfM digital elevation models to estimate lavaka (gully) volumes and mobilization rates in the Lake Alaotra region (Madagascar). *Earth Surface Dynamics* 10(2): 209–227. <https://doi.org/10.5194/esurf-10-209-2022>
- Bueso-Bello J-L, Martone M, González C, Sica F, Valdo P, Posovszky P, Pulella A, Rizzoli P (2021) The Global Water Body Layer from TanDEM-X Interferometric SAR Data. *Remote Sensing* 13 (24): 5069. <https://doi.org/10.3390/rs13245069>
- Carrera-Hernández JJ (2021) Not all DEMs are equal: An evaluation of six globally available 30 m resolution DEMs with geodetic benchmarks and LiDAR in Mexico. *Remote Sensing of Environment* 261: 112474. <https://doi.org/10.1016/j.rse.2021.112474>
- CloudCompare project (2025) CloudCompare <https://www.cloudcompare.org/> [Accessed on 16.09.2025]
- Dimitrov D, Nyagolov I, Balabanova S, Lisev N, Koshinchanov G, Korcheva A, Marinski Y, Pashova L, Grozdev D, Vasilev V, Bozhilov B, Tsvetkova N (2013) Metodika za otsenka na zaplahata i riska ot navodnenia, saglasno iziskvaniyata na Direktiva 2007/60/ES [Methods for assessment of flood hazard and flood risk, according to requirements of the EU Floods Directive 2007/60]. Contract No D-30-62.
- Dinkov D (2023) Accuracy assessment of high-resolution terrain data produced from UAV images georeferenced with on-board PPK positioning. *Journal of the Bulgarian Geographical Society* 48: 43–53. <https://doi.org/10.3897/jbgs.e89878>
- Directive 2007/60 (2007) Directive (EU) 2007/60/EC of the European Parliament and of the Council of October 23, 2007, on the assessment and management of flood risks. *Official Journal of the European Union*, L 288/27, 06.11.2007. <http://data.europa.eu/eli/dir/2007/60/oj> [Accessed on 17.08.2025]

- Emmendorfer IB, De Almeida LPM, Alves DCL, Emmendorfer LR, Arigony-Neto J (2024) Accuracy assessment of global DEMs for the mapping of coastal flooding on a low-lying sandy environment: Cassino Beach, Brazil. *Regional Studies in Marine Science* 74: 103535. <https://doi.org/10.1016/j.rsma.2024.103535>
- EOC Geoservice (2025) TanDEM-X - Edited Digital Elevation Model (EDEM) - Global, 30m https://download.geoservice.dlr.de/TDM30_EDEM/ [Accessed on 30.11.2024]
- EU-DEM (2022) COPERNICUS Digital Elevation Model (DEM) for Europe at 30 meter resolution (EU-LAEA) derived from Copernicus Global 30 meter dataset. <https://data.opendatascience.eu/geonetwork/srv/api/records/9a382836-47a9-4dac-ad62-f0021e455ab8> [Accessed on 21.08.2025]
- Fazeli H, Samadzadegan F, Dadrasjavan F (2016) Evaluating the potential of RTK-UAV for automatic point cloud generation in 3D rapid mapping. *ISPRS - International Archives of the Photogrammetry, Remote Sensing and Spatial Information Sciences XLI-B6*: 221–226. <https://doi.org/10.5194/isprsarchives-XLI-B6-221-2016>
- GCCA [Geodesy, Cartography and Cadastre Agency] (2023) Geocartfund <https://www.cadastre.bg/en/geokartfond> [Accessed on 03.08.2023]
- GCCA [Geodesy, Cartography and Cadastre Agency] (2025) BGSTrans 4.6 Coordinate Transformation Program <https://www.cadastre.bg/programa-za-transformaciya-na-koordinati-bgstrans-45> [Accessed on 10.08.2025]
- Gesch D (2023) Assessing Global Elevation Models for Mapping the Low Elevation Coastal Zone. In: Niculiță M, Guth P, Reuter H, Lecours V, Grohmann C, Arundel S, Qin C-Z (Eds) *Geomorphometry 2023 Proceedings. 7th International Conference on Geomorphometry, Geomorphometry 2023, Iași (Romania), July 2023*. Tehnopress, Iași, 11–13. <https://doi.org/10.5281/ZENODO.8011577>
- González C, Bachmann M, Bueso-Bello J-L, Rizzoli P, Zink M (2020) A Fully Automatic Algorithm for Editing the TanDEM-X Global DEM. *Remote Sensing* 12(23): 3961. <https://doi.org/10.3390/rs12233961>
- Greenwalt C, Schultz ME (1962) *Principles of Error Theory and Cartographic Applications*. Aeronautical Chart and Information Center, St Louis, Missouri <https://apps.dtic.mil/sti/tr/pdf/AD0276978.pdf> [Accessed on 12.06.2025]
- Guth PL, Trevisani S, Grohmann CH, Lindsay J, Gesch D, Hawker L, Bielski C (2024) Ranking of 10 Global One-Arc-Second DEMs Reveals Limitations in Terrain Morphology Representation. *Remote Sensing* 16(17): 3273. <https://doi.org/10.3390/rs16173273>
- Guth PL, Van Niekerk A, Grohmann CH, Muller J-P, Hawker L, Florinsky IV, Gesch D, Reuter HI, Herrera-Cruz V, Riazanoff S, López-Vázquez C, Carabajal CC, Albinet C, Strobl P (2021) Digital Elevation Models: Terminology and Definitions. *Remote Sensing* 13(18): 3581. <https://doi.org/10.3390/rs13183581>
- Hawker L, Bates P, Neal J, Rougier J (2018a) Perspectives on Digital Elevation Model (DEM) Simulation for Flood Modeling in the Absence of a High-Accuracy Open Access Global DEM. *Frontiers in Earth Science* 6: 233. <https://doi.org/10.3389/feart.2018.00233>
- Hawker L, Rougier J, Neal J, Bates P, Archer L, Yamazaki D (2018b) Implications of Simulating Global Digital Elevation Models for Flood Inundation Studies. *Water Resources Research* 54(10): 7910–7928. <https://doi.org/10.1029/2018WR023279>
- Hawker L, Neal J, Bates P (2019) Accuracy assessment of the TanDEM-X 90 Digital Elevation Model for selected floodplain sites. *Remote Sensing of Environment* 232: 111319. <https://doi.org/10.1016/j.rse.2019.111319>

- Hawker L, Uhe P, Paulo L, Sosa J, Savage J, Sampson C, Neal J (2022) A 30 m global map of elevation with forests and buildings removed. *Environmental Research Letters* 17(2): 024016. <https://doi.org/10.1088/1748-9326/ac4d4f>
- Höhle J, Höhle M (2009) Accuracy assessment of digital elevation models by means of robust statistical methods. *ISPRS Journal of Photogrammetry and Remote Sensing* 64(4): 398–406. <https://doi.org/10.1016/j.isprsjprs.2009.02.003>
- Iheaturu CJ, Ayodele EG, Okolie CJ (2020) An assessment of the accuracy of structure-from-motion (SfM) photogrammetry for 3D terrain mapping. *Geomatics, Land-management and Landscape* 2:65–82. <https://doi.org/10.15576/GLL/2020.2.65>
- Iqbal U, Riaz MZB, Zhao J, Barthelemy J, Perez P (2023) Drones for Flood Monitoring, Mapping and Detection: A Bibliometric Review. *Drones* 7(1): 32. <https://doi.org/10.3390/drones7010032>
- Jongman B, Ward PJ, Aerts JCJH (2012) Global exposure to river and coastal flooding: Long term trends and changes. *Global Environmental Change* 22(4): 823–835. <https://doi.org/10.1016/j.gloenvcha.2012.07.004>
- Kakoulaki G, Martinez Fernandez AM, Florio P (2021) Non-commercial Light Detection and Ranging (LiDAR) data in Europe, EUR 30817 EN. Publications Office of the European Union, Luxembourg. <https://doi.org/10.2760/212427>
- Karamuz E, Romanowicz RJ, Doroszkiewicz J (2020) The use of unmanned aerial vehicles in flood hazard assessment. *Journal of Flood Risk Management* 13(4): e12622. <https://doi.org/10.1111/jfr3.12622>
- Kulp S, Strauss BH (2016) Global DEM Errors Underpredict Coastal Vulnerability to Sea Level Rise and Flooding. *Frontiers in Earth Science* 4:36. <https://doi.org/10.3389/feart.2016.00036>
- Kulp SA, Strauss BH (2018) CoastalDEM: A global coastal digital elevation model improved from SRTM using a neural network. *Remote Sensing of Environment* 206: 231–239. <https://doi.org/10.1016/j.rse.2017.12.026>
- Lee J-Y, Hong S-H (2024) Construction of Digital Elevation Models on the Intertidal Flats Using TanDEM-X Bistatic Observations. *IEEE Geoscience and Remote Sensing Letters* 21: 1–5. <https://doi.org/10.1109/LGRS.2024.3370258>
- Li Y, Wu Y, Sun Z, Zhao D, Yu C, Li Y, You G, Kong Z, Xi X, Lei L (2023) Using UAV imagery to generate DEMs of the intertidal zone. *Journal of Coastal Conservation* 27(3): 23. <https://doi.org/10.1007/s11852-023-00951-1>
- MAF [Ministry of Agriculture and Food] (2024) Digital orthophoto map https://www.mzh.government.bg/media/filer_public/2025/01/16/ad_2024_en.pdf [Accessed on 05.06.2025]
- Meadows M, Jones S, Reinke K (2024) Vertical accuracy assessment of freely available global DEMs (FABDEM, Copernicus DEM, NASADEM, AW3D30 and SRTM) in flood-prone environments. *International Journal of Digital Earth* 17(1): 2308734. <https://doi.org/10.1080/17538947.2024.2308734>
- MD [Ministry of Defence] Portal (2025) Geoportal of Ministry of Defence <https://gis.armf.bg/en/Services> [Accessed on 20.08.2023]
- MOEW [Ministry of Environment and Water] (2016) Bulgarian Ramsar Sites https://www.moew.government.bg/static/media/ups/tiny/filebase/Nature/Natura%202000/RAMSAR/Ramsar_2016.pdf [Accessed on 05.06.2025]
- MOEW [Ministry of Environment and Water] (2021) Natsionalnata metodika za kartirane na zaplahata i riska ot navodnenia (aktualizatsia) [National methodology for flood hazard and risk mapping (Updated version)] <https://www.moew.government.bg/stat->

- [ic/media/ups/tiny/filebase/Water/PURN/PURN%202022-2027/Final%20FHRM%20methodology.pdf](#) [Accessed on 17.07.2025]
- MOEW [Ministry of Environment and Water] (2021) Predvaritelna otsenka na riska ot navodnenia za Chernomorski rayon za baseynovo upravlenie. Prilozhenie 2: Izpolzvani danni za izgotvyane na PORN [Preliminary Flood Risk Assessment for the Black Sea Basin Management Region. Annex 2: Data used for the preparation of the PORN. https://www.bsbd.bg/PURN/2022-2027/02_PFRA_BG2_APP02_sourcesOfInformation.pdf [Accessed on 25.02.2025]
- MOEW [Ministry of Environment and Water] (2023) Plan za upravlenie na riska ot navodnenia za perioda 2022-2027 za Chernomorski rayon za baseynovo upravlenie [Flood Risk Management Plan for the period 2022-2027 for the Black Sea Basin Management Region] https://www.bsbd.bg/PURN/2022-2027/final/BG2_FRMP.pdf [Accessed on 17.07.2025]
- MRDPW [Ministry of Regional Development and Public Works] (2011) Instruction No. RD-02-20-25 of September 20, 2011, on the Determination of Geodetic Points Using Global Navigation Satellite Systems. State Gazette – the Official Journal of the Republic of Bulgaria 79, 11.10.2011. [Accessed on 17.08.2025]
- Nicholls R, Zanuttigh B, Vanderlinden JP, Weisse R, Silva R, Hanson S, Narayan S, Hoggart S, Thompson RC, Vries WD, Koundouri P (2015) Developing a Holistic Approach to Assessing and Managing Coastal Flood Risk. In: Coastal Risk Management in a Changing Climate. Elsevier, 9–53. <https://doi.org/10.1016/B978-0-12-397310-8.00002-6>
- Nikolov G (2018) TsMR za teritoriyata na Bulgaria – razvitie i prilozhenia [DEM for the territory of Bulgaria – development and applications]. In: Proceedings of XXVIII International symposium on Modern technologies, education and professional practice in geodesy and related fields, Sofia (Bulgaria), November 2018. <https://symp2018.geodesy-union.org/wp-content/uploads/2018/11/23.pdf>
- Oppenheimer M, Glavovic BC, Hinkel J, van de Wal R, Magnan AK, Abd-Elgawad A, Cai R, Cifuentes-Jara M, DeConto RM, Ghosh T, Hay J, Isla F, Marzeion B, Meyssignac B, Sebesvari Z (2019) Sea Level Rise and Implications for Low-Lying Islands, Coasts and Communities. In: [Pörtner H-O, Roberts DC, Masson-Delmotte V, Zhai P, Tignor M, Poloczanska E, Mintenbeck K, Alegría A, Nicolai M, Okem A, Petzold J, Rama B, Weyer NM (Eds) IPCC Special Report on the Ocean and Cryosphere in a Changing Climate. Cambridge University Press, Cambridge, UK and New York, NY, USA, 321–445. <https://doi.org/10.1017/9781009157964.006>
- Pashova L, Kortcheva A, Galabov V (2017) On the Necessity of Improving the Research Infrastructure in the Western Black Sea for the Purposes of Flood Risk Management. In: Nikolov O, Veeravalli S (Eds), Implications of Climate Change and Disasters on Military Activities. NATO Science for Peace and Security Series C: Environmental Security. Springer Netherlands, Dordrecht, 31–46. https://doi.org/10.1007/978-94-024-1071-6_7
- Pashova L, Nikolov G (2018) DEM testing using GNSS measurements in SW Bulgaria. Annual of the University of architecture, civil engineering and geodesy 51(9): 97–107. https://annual.uacg.bg/article/2018_51_9_08
- Petrov D (2013) Bazi danni za relefa na teritoriyata na Republika Bulgaria sazdadeni po topografski karti 1:50000 i 1:25000 [Databases for the relief of the territory of the Republic of Bulgaria created on topographic maps 1:50000 and 1:25000]. Magazine Geomedia <https://www.geomedia.bg/geodesia/bazi-danni-za-relefa-na-teritoriyata-na/> [Accessed on 04.06.2025]

- Pix4D (2020) Pix4D Mapper 4.5.6 software <https://www.pix4d.com/> [Accessed on 26.07.2025]
- Planchon O, Darboux F (2002) A fast, simple and versatile algorithm to fill the depressions of digital elevation models. *CATENA* 46(2–3): 159–176. [https://doi.org/10.1016/S0341-8162\(01\)00164-3](https://doi.org/10.1016/S0341-8162(01)00164-3)
- Prodanov B, Kotsev I, Lambev T, Bekova R (2020) Unmanned Aerial Vehicles for Surveying the Bulgarian Black Sea Coast. *Comptes rendus de l'Academie Bulgare des Sciences* 73(5): 666–672 <https://doi.org/10.7546/CRABS.2020.05.09>
- Prodanov B, Dimitrov L, Kotsev I, Bekova R, Lambev T (2023) Spatial distribution of sand dunes along the Bulgarian Black Sea Coast: inventory, UAS mapping and new discoveries. *Nature Conservation* 54: 81–120. <https://doi.org/10.3897/natureconservation.54.105507>
- Pronk M, Hooijer A, Eilander D, Haag A, De Jong T, Voudoukas M, Vernimmen R, Ledoux H, Eleveld M (2024) DeltaDTM: A global coastal digital terrain model. *Scientific Data* 11(1): 273. <https://doi.org/10.1038/s41597-024-03091-9>
- QGIS Association (2023) QGIS 3.34 LTR [Accessed on 05.08.2025]
- Black Sea Basin Directorate (2024) River Basin Management Plans and Flood Risk Management Plans, <https://www.bsbd.bg/> [Accessed on 18.11.2025]
- Schumann G, Bates PD, Apel H, Aronica GT (2018) Global Flood Hazard Mapping, Modeling, and Forecasting: Challenges and Perspectives. In: Schumann GJ, Bates PD, Apel H, Aronica GT (Eds), *Geophysical Monograph Series*. Wiley, 239–244. <https://doi.org/10.1002/9781119217886.ch14>
- Shen P, Wei S, Shi H, Gao L, Zhou W-H (2023) Coastal Flood Risk and Smart Resilience Evaluation under a Changing Climate. *Ocean-Land-Atmosphere Research* 2: 0029. <https://doi.org/10.34133/olar.0029>
- Specht M, Wiśniewska M (2024) A Method for Developing a Digital Terrain Model of the Coastal Zone Based on Topobathymetric Data from Remote Sensors. *Remote Sensing* 16(24): 4626. <https://doi.org/10.3390/rs16244626>
- Sun S, Xue Q, Xing X, Zhao H, Zhang F (2024) Remote Sensing Image Interpretation for Coastal Zones: A Review. *Remote Sensing* 16(24): 4701. <https://doi.org/10.3390/rs16244701>
- Turner IL, Harley MD, Drummond CD (2016) UAVs for coastal surveying. *Coastal Engineering* 114: 19–24. <https://doi.org/10.1016/j.coastaleng.2016.03.011>
- Uuemaa E, Ahi S, Montibeller B, Muru M, Kmoch A (2020) Vertical Accuracy of Freely Available Global Digital Elevation Models (ASTER, AW3D30, MERIT, TanDEM-X, SRTM, and NASADEM). *Remote Sensing* 12(21): 3482. <https://doi.org/10.3390/rs12213482>
- Uysal M, Toprak AS, Polat N (2015) DEM generation with UAV Photogrammetry and accuracy analysis in Sahitler hill. *Measurement* 73: 539–543. <https://doi.org/10.1016/j.measurement.2015.06.010>
- Van De Sande B, Lansen J, Hoyng C (2012) Sensitivity of Coastal Flood Risk Assessments to Digital Elevation Models. *Water* 4(3): 568–579. <https://doi.org/10.3390/w4030568>
- Velegrakis AF, Chatzistratis D, Chalazas T, Armaroli C, Schiavon E, Alves B, Grigoriadis D, Hasiotis T, Ieronymidi E (2024) Earth observation technologies, policies and legislation for the coastal flood risk assessment and management: a European perspective. *Anthropocene Coasts* 7(1): 3. <https://doi.org/10.1007/s44218-024-00037-x>
- Weil J (1986) The synthesis of cloth objects. In: *Proceedings of the 13th annual conference on Computer graphics and interactive techniques*. ACM, 49–54. <https://doi.org/10.1145/15922.15891>

- Wessel B (2016) TanDEM-X Ground Segment – DEM Products Specification Document. EOC, DLR, Oberpfaffenhofen, Germany, Public Document TD-GS-PS-0021, Issue 3.1. <https://tandemx-science.dlr.de> [Accessed on 15.06.2025]
- Wessel B, Huber M, Wohlfart C, Marschalk U, Kosmann D, Roth A (2018) Accuracy assessment of the global TanDEM-X Digital Elevation Model with GPS data. *ISPRS Journal of Photogrammetry and Remote Sensing* 139: 171–182. <https://doi.org/10.1016/j.isprsjprs.2018.02.017>
- Wise S (2000) Assessing the quality for hydrological applications of digital elevation models derived from contours. *Hydrological Processes* 14(11–12): 1909–1929. [https://doi.org/10.1002/1099-1085\(20000815/30\)14:11/12%253C1909::AID-HYP45%253E3.0.CO;2-6](https://doi.org/10.1002/1099-1085(20000815/30)14:11/12%253C1909::AID-HYP45%253E3.0.CO;2-6)
- Yap BW, Sim CH (2011) Comparisons of various types of normality tests. *Journal of Statistical Computation and Simulation* 81(12): 2141–2155. <https://doi.org/10.1080/00949655.2010.520163>
- Zhang K, Gann D, Ross M, Biswas H, Li Y, Rhome J (2019) Comparison of TanDEM-X DEM with LiDAR Data for Accuracy Assessment in a Coastal Urban Area. *Remote Sensing* 11(7): 876. <https://doi.org/10.3390/rs11070876>
- Zhang W, Qi J, Wan P, Wang H, Xie D, Wang X, Yan G (2016) An Easy-to-Use Airborne LiDAR Data Filtering Method Based on Cloth Simulation. *Remote Sensing* 8(6): 501. <https://doi.org/10.3390/rs8060501>
- Zink M, Bachmann M, Brautigam B, Fritz T, Hajnsek I, Moreira A, Wessel B, Krieger G (2014) TanDEM-X: The New Global DEM Takes Shape. *IEEE Geoscience and Remote Sensing Magazine* 2(2): 8–23. <https://doi.org/10.1109/MGRS.2014.2318895>

Additional information

Conflict of interest

No conflict of interest was declared.

Ethical statement

No ethical statement was reported.

Use of AI

No use of AI was reported.

Funding

The study was funded by the Bulgarian Scientific Research Fund under Contract KP-06-COST/8, 25.09.2020.

Author contributions

Conceptualization: DD, LP. Methodology: DD, LP. Software: DD, LP. Validation: DD. Formal analysis: DD, LP. Investigation: DD, LP. Resources: DD, LP. Data Curation: DD, LP. Writing - Original draft: DD, LP. Writing - Review and Editing: LP, DD. Visualization: DD. Project administration: LP. Funding Acquisition: LP.

Author ORCIDs

Davis Dinkov  <https://orcid.org/0000-0001-5592-636X>

Lyubka Pashova  <https://orcid.org/0000-0002-8058-9905>

Data availability

A free version of the TanDEM-X 30 m digital elevation is available via EOC Geoservice (https://download.geoservice.dlr.de/TDM30_EDEM/, last access: November 30, 2024). BG DSM 4 m and topographic data are provided free of charge by the Ministry of Agriculture and Land and the Agency of Geodesy, Cartography, and Cadaster. MGS DEM 10 m is provided by the Military Geographical Service of the Bulgarian Army upon paid request. All DEMs can be provided upon appropriate request addressed to the corresponding author.